DIGITAL SIMULATION OF RANDOM VIBRATIONS

By
DONALD JOSEPH BELZ

A DISSERTATION PRESENTED TO THE GRADUATE COUNCIL OF
THE UNIVERSITY OF FLORIDA
IN PARTIAL FULFILLMENT OF THE REQUIREMENTS FOR THE
DEGREE OF DOCTOR OF PHILOSOPHY

UNIVERSITY OF FLORIDA
December, 1964

ACKNOWLEDGMENTS

The author wishes to express his thanks and appreciation to Dr. William A. Nash, Chairman of his Supervisory Committee, for encouraging him to undertake the present study and for guidance throughout the course of this investigation.

He also wishes to express his gratitude to Professors R. G. Blake, I. K. Ebcioglu, A. Jahanshahi, J. Siekmann, and the late Professor H. A. Meyer, for having served on his Supervisory Committee.

Finally, the author wishes to acknowledge the Air Force Office of Scientific Research for their sponsorship of the work.

TABLE OF CONTENTS

		Page
ACKNOWLEDGMENTS		ii
LIST OF TABLES		v
LIST OF FIGURES		vi
NOMENCLATURE		x
ABSTRACT		xii
Chapter		
I.	INTRODUCTION	1
II.	SIMULATION OF A RANDOM FORCING FUNCTION	5
	2.1 Random Numbers and Pseudo-Random Numbers	5
	2.2 Statistical Background	8
	2.3 Gaussian Random Number Generation	12
	2.4 Autocorrelated Random Function Simulation	17
III.	MATHEMATICAL MODEL OF THE BERNOULI-EULER BEAM INCLUDING THE EFFECTS OF FINITE LATERAL DEFLECTION AND STRETCHING OF THE MIDDLE SURFACE	27
	3.1 Equation of Motion Under Transverse Loads	27
	3.2 Boundary and Initial Conditions	34
IV.	DEFLECTION REPONSE OF BEAMS TO DETERMINISTIC AND CORRELATED RANDOM FORCING FUNCTIONS	38
	4.1 Deflection Response for a Concentrated Load of Constant Magnitude Suddenly Applied at Midspan	38
	4.2 Statistical Response to a Time-Random Concentrated Load Applied at Midspan	44

Chapter Page

V. CONCLUSIONS 92

APPENDIX 94

Digital Computer Program: 'Simulation; Random Vibrations of Beams' 95

LIST OF REFERENCES 102

BIOGRAPHICAL SKETCH. 104

LIST OF TABLES

Table		Page
1.	Distribution of 1124 Elements of the "Basic Set"	14
2.	Numerical Values of Beam Parameters.	40

LIST OF FIGURES

Figure		Page
1.	Normalized autocorrelation functions of F(t) for T/δt = 500,...,4500	23
2.	Comparison of autocorrelation functions $\bar{R}_E$ and $\bar{R}_P$	25
3.	Deflection response for a concentrated load of 25 lb. applied suddenly at midspan	41
4.	Nonlinear deflection response for a concentrated load of 12,500 lb. applied suddenly at midspan	42
5.	Nonlinear deflection response (σ_p = 1,000#, ends pinned)	45
6.	Nonlinear deflection response (σ_p = 5,000#, ends pinned)	46
7.	Nonlinear deflection response (σ_p = 10,000#, ends pinned)	47
8.	Nonlinear deflection response (σ_p = 15,000#, ends pinned)	48
9.	Nonlinear deflection response (σ_p = 20,000#, ends pinned)	49
10.	Linear deflection response (σ_p = 20,000#, ends pinned)	50
11.	Nonlinear deflection response (σ_p = 1,000#, ends fixed)	51
12.	Nonlinear deflection response (σ_p = 5,000#, ends fixed)	52
13.	Nonlinear deflection response (σ_p = 10,000#, ends fixed)	53
14.	Nonlinear deflection response (σ_p = 15,000#, ends fixed)	54

Figure Page

15. Nonlinear deflection response (σ_p = 20,000#, ends fixed) 55

16. Linear deflection response (σ_p = 20,000#, ends fixed) 56

17. Excitation and response standard deviations (ends pinned) 58

18. Excitation and response standard deviations (ends fixed). 59

19. Nonlinear-response probability density functions (σ_p = 10,000#, ends pinned) 60

20. Nonlinear-response probability density functions(σ_p = 15,000#, ends pinned). 61

21. Nonlinear-response probability density functions (σ_p = 20,000#, ends pinned) 62

22. Linear-response probability density functions (σ_p = 20,000#, ends pinned) 63

23. Nonlinear-response probability density functions (σ_p = 20,000#, ends fixed). 64

24. Linear-response probability density function (σ_p = 20,000#, ends fixed). 65

25. Nonlinear-response autocorrelation functions (σ_p = 1,000#, ends pinned). 66

26. Nonlinear-response autocorrelation functions (σ_p = 5,000#, ends pinned). 67

27. Nonlinear-response autocorrelation functions (σ_p = 10,000#, ends pinned) 68

28. Nonlinear-response autocorrelation functions (σ_p = 15,000#, ends pinned) 69

29. Nonlinear-response autocorrelation functions (σ_p = 20,000#, ends pinned) 70

30. Linear-response autocorrelation functions (σ_p = 20,000#, ends pinned) 71

Figure		Page
31.	Nonlinear-response autocorrelation functions (σ_p = 1,000#, ends fixed)	72
32.	Nonlinear-response autocorrelation functions (σ_p = 5,000#, ends fixed)	73
33.	Nonlinear-response autocorrelation functions (σ_p = 10,000#, ends fixed)	74
34.	Nonlinear-response autocorrelation functions (σ_p = 15,000#, ends fixed)	75
35.	Nonlinear-response autocorrelation functions (σ_p = 20,000#, ends fixed)	76
36.	Linear-response autocorrelation functions (σ_p = 20,000#, ends fixed)	77
37.	Nonlinear-response power spectra (σ_p = 1,000#, ends pinned)	78
38.	Nonlinear-response power spectra (σ_p = 5,000#, ends pinned)	79
39.	Nonlinear-response power spectra (σ_p = 10,000#, ends pinned)	80
40.	Nonlinear-response power spectra (σ_p = 15,000#, ends pinned)	81
41.	Nonlinear-response power spectra (σ_p = 20,000#, ends pinned)	82
42.	Linear-response power spectra (σ_p = 20,000#, ends pinned)	83
43.	Nonlinear-response power spectra (σ_p = 1,000#, ends fixed)	84
44.	Nonlinear-response power spectra (σ_p = 5,000#, ends fixed)	85
45.	Nonlinear-response power spectra (σ_p = 10,000#, ends fixed)	86
46.	Nonlinear-response power spectra (σ_p = 15,000#, ends fixed)	87

Figure Page

47. Nonlinear-response power spectra (σ_p = 20,000#, ends fixed) 88

48. Linear-response power spectra (σ_p = 20,000#, ends fixed). 89

NOMENCLATURE

Symbol	Definition
A	Cross-sectional area
b	Word size of a digital computer
B_i	i^{th} element of the "basic set" of random numbers
E	Modulus of elasticity
$f(v)$	Probability density function of the random variable v
$F(t)$	Simulated time-random function
h	Thickness of beam
K	Viscous damping coefficient; also a constant in the power residue method
K_E	Equivalent linear spring constant
L	Length of beam
$P(t)$	Time-dependent concentrated load
q	Lateral surface load
$R(\tau)$	Autocorrelation function
R_o	Linear correlation coefficient
$S(\omega)$	Power spectral density as a function of angular frequency
S_i	i^{th} pseudo-random number in the set S
t	Time
v	A random variable
$V(t)$	A random function

NOMENCLATURE -- Continued

Symbol	Definition
w	Lateral deflection of a beam
x,y,z	Rectangular coordinates
$\delta t, \Delta t$	Finite increments of time
Δx	Finite increment of x
μ	Mean
ρ	Mass density
σ	Standard deviation
σ_{ij}	Components of stress
τ	Time delay
ϕ	Gaussian probability density function
ω	Angular frequency in radians per second

Abstract of Dissertation Presented to the Graduate Council in Partial Fulfillment of the Requirements for the Degree of Doctor of Philosophy

DIGITAL SIMULATION OF RANDOM VIBRATIONS

by

Donald Joseph Belz

December, 1964

Chairman: Dr. William A. Nash
Major Department: Engineering Science and Mechanics

A physically realizable stationary, Gaussian, random load is simulated digitally and employed as the forcing function in the equation of motion of a damped, elastic beam whose resistance to deformation is due to bending and stretching. Rotations are considered to be finite, the squares of slopes being negligible compared with unity, but of the order of magnitude of linearized strains. The power residue method for generating pseudo-random numbers is employed in the technique presented for constructing the random function, whose statistical properties correspond closely to those of pressure signals measured in the noise field of a turbulent subsonic air jet.

The nonlinear equation of motion for the beam is written in finite difference form and programmed together with the random load simulation in FORTRAN (709) for

solution on a digital computer. The forcing function used represents a time-random concentrated load applied transversely at midspan. Boundary conditions used include rotationally fixed and pinned ends.

Numerical solutions are obtained, from which statistical measures of response at midspan and at the quarter points of the beam are computed. Response autocorrelation functions, power spectra, and probability density functions are presented graphically for a range of load mean-square values. The variation of mean-square load with mean square response is also shown and compared with the corresponding linear relation.

Although the technique used in the present study was applied to the problem of a beam carrying a time-random concentrated load, it can in principle be applied to more complicated structural components and random load configurations.

CHAPTER I

INTRODUCTION

During the last decade, increasing attention has been given to the problem of predicting the response of structures to random excitation (1,2). Practical motivation for such research has arisen primarily in the field of aircraft, missile, and space vehicle development.

In the powered phase of missile or launch-vehicle flight, both the missile structure and payload are subjected to random excitation of high intensity. The response of the total system to such loads can be a determining factor in the success or failure of a mission. Vibration-sensitive equipment, when carried aloft, can fail to perform properly if the vibrational environment is too severe; over a sufficiently long operating life, random excitations can contribute to the fatigue failure of a structural component.

The earliest analyses of the response of structures to random loads were concerned with linear structures, i.e. those having linear differential equations of motion (1). Physical structures, however, are not always so obliging

as to respond to excitation in a manner consistent with linear theory.

In particular, continuous elastic structural elements, e.g. beams, plates, and shells, can exhibit large (finite) deflections, in which case the governing equations of motion may be nonlinear.

An approximate technique, known as the method of "equivalent linearization" has been developed and applied to several mechanical problems (3). The method is inherently limited to the class of problems having small nonlinearities.

An exact technique (4) is available for determining an integral representation of a nonlinear structural response when the excitation can be represented as a Markov process. This approach has been applied to beams and plates with nonlinearities arising from finite, moderately large slopes of the middle surface (5). The restriction that an applied load must be characterized as a Markov process prohibits the use of this technique for random loads that are continuous functions of spacial coordinates or time. Successive values of a Markov process are statistically uncorrelated, implying a physically unrealizable power spectrum (white noise) and an infinite mean square.

Because analytical approaches for predicting the response of nonlinear structures to correlated random loads are totally lacking, methods of numerical analysis were employed in the present study to simulate both a structural element and a continuous (correlated) random forcing function.

Numerical techniques for solving partial differential equations, both linear and nonlinear in form, have been available for many years (6). The application of such techniques has of late been rendered practicable by the existence of high speed digital computers. But before such techniques can be employed in a study of random vibrations, it is necessary that a sequence of random numbers, representing a desired forcing function, be made available. The present study was therefore initially concerned with the development of an efficient means of simulating physically realizable random loads in a form directly usable in a digital computer. (That method of simulation is described in Chapter II.) The structural model chosen for investigation was that of a beam whose resistance to deformation arises from bending and stretching. The response of such a beam to transverse loading, for moderately large slopes of the middle surface, is linear when the ends are unrestrained against longitudinal translation and nonlinear when both ends are restrained

against longitudinal translation. Both cases were considered, with the forcing function in the form of a concentrated, time-random load at midspan, and boundary conditions corresponding to rotationally unrestrained ends and rotationally fixed ends.

CHAPTER II

SIMULATION OF A RANDOM FORCING FUNCTION

Physical loads associated with continuous structures are most generally functions of time and spatial coordinates. For simplicity, this chapter is concerned with the simulation of a continuous, Gaussian, random function, F, of one variable, t. The method employed can, by direct extension, be applied to simulate continuous, Gaussian, random functions of a finite number of variables.

Before proceeding to a description of the random load simulation, those statistical and related concepts basic to the analysis will be considered briefly.

2.1. Random numbers and Pseudo-Random Numbers

Under its classical definition, a set of random numbers is distinguished not so much by its properties as by its historical origin (7). Random numbers are numbers assigned to the elements of a sample space which in turn are defined as the possible outcomes of some chance event or experiment (8). For example, a gambler's die has six faces distinguished by dots corresponding to the numbers one through six. If the die is true and "fairly" tossed,

each face has an equal probability of being on top when the die comes to rest. (The probability that a particular outcome will occur in a given experiment is the number of results corresponding to that outcome divided by the total number of possible results.) Thus, for a perfect die given a fair toss, the number of dots on the top face, when the die comes to rest, is by definition a random number. Random numbers then can be generated by gambling devices (to the extent that such devices are unbiased) or by physical processes such as radioactive decay. It is thus possible to generate and store, in printed tables or on punched cards, large sequences of random numbers.

As a practical matter, however, it is often inconvenient to use such tables or cards when high speed digital computers are employed. A less time consuming, and therefore more efficient, procedure is for the computer to generate, deterministically, a set of numbers which are operationally random, i.e. which are indistinguishable from random numbers under statistical tests of randomness. Such numbers have been given the name "pseudo-random numbers" (9). Hereafter we shall no longer be concerned with random numbers, but only with pseudo-random numbers. To avoid a cumbersome phrase, pseudo-random numbers will henceforth be referred to simply as random numbers.

Many methods have been devised for generating such random numbers. One of the most successful, called the power residue method (9,10), was employed in the present study.

The following is, in brief, the power residue method. Let S_0 be any odd integer. Let

$$S_i = K S_{i-1} \quad (2.1)$$

If b is the word size of a binary computer, K is chosen such that $K \simeq 2^{b/2}$. Calculation of KS_0 produces a product $2b$ bits long. The multiplication, performed with double precision, permits the b least significant digits to be retained as the next random integer, while the b higher bits are discarded. The sequence of random integers generated by continuation of this procedure are converted to a set of random numbers (called the "basic set") which are distributed uniformly over the unit interval bounded from below by zero, by floating the random integers and establishing a decimal point to the immediate left of each integer.

The sequence of numbers thus obtained will eventually repeat itself, i.e. the sequence is periodic. However, the 35 bit word length of the IBM709 computer used in this study permits a sequence with a period of "over 8.5 billion numbers" to be generated (10). Thus, the periodicity of those numbers was ignored.

2.2 Statistical Background

Let $V(t)$ be a function generated by a random or "chance" process. The value of the function at any $t = t_o$ is thus a random variable, $-\infty < v < +\infty$. Associated with v is a function $f(v)$, which for v continuous is defined such that

$$f(v) \geq 0, \tag{2.2}$$

$$\int_{-\infty}^{\infty} f(v)\,dv = 1, \tag{2.3}$$

$$\int_{a}^{b} f(v)\,dv = P\{a \leq v \leq b\}, \tag{2.4}$$

where a and b are any two values of v, with $b > a$, and $P\{a \leq v \leq b\}$ is the probability that v lies within the closed interval bounded by a and b. The function $f(v)$ is called the probability density function of v.

The mean of v, denoted by μ_v is defined as

$$\mu_v = \int_{-\infty}^{\infty} v\, f(v)\,dv. \tag{2.5}$$

The mean is a measure of the central tendency of v.

The r^{th} central moment of v is defined as

$$\mu_v^r = \int_{-\infty}^{\infty} (v - \mu_v)^r f(v)\,dv. \tag{2.6}$$

The averages indicated in definitions (2.5) and (2.6) are designated ensemble averages. Of particular statistical interest is the second central moment ($r = 2$), commonly called the variance, which is a measure of dispersion about the mean. The square root of the variance is designated standard deviation. When $\mu_V = 0$ in expression (2.6), the variance is called the mean square.

The function V(t) may also be averaged over t . If V(t) is continuous and defined for $-\infty < t < +\infty$, then

$$(2.7) \qquad \bar{\mu}_V = \lim_{|T| \to \infty} \frac{1}{2T} \int_{-T}^{T} V(t)\, dt \ ,$$

$$(2.8) \qquad \bar{\mu}_V^r = \lim_{|T| \to \infty} \frac{1}{2T} \int_{-T}^{T} \left[V(t) - \bar{\mu}_V \right]^r dt \ ,$$

and, in particular,

$$(2.9) \qquad \sigma_V^2 = \bar{\mu}_V^2 = \lim_{|T| \to \infty} \frac{1}{2T} \int_{-T}^{T} \left[V(t) - \bar{\mu}_V \right]^2 dt \ ,$$

where a bar indicates averaging over the range of t .

A function, V(t), is said to be stationary if averages over t , with /T/ finite and sufficiently large, are independent of the location of the origin $t = 0$.

A stationary random function may also be ergodic. A random function, V(t), for which averages over the range

of t equal the corresponding ensemble averages, is said to be ergodic. The significance of ergodicity is that any member of the ensemble of an ergodic process is statistically typical of the ensemble. (It is of value to note that every random process that is stationary and has zero mean, Gaussian probability density function, and a continuous autocorrelation function is also ergodic.)

The autocorrelation function of V(t) is defined as

$$(2.10) \qquad \bar{R}_V(\tau) = \lim_{|T|\to\infty} \frac{1}{2T} \int_{-T}^{T} V(t)\, V(t+\tau)\, dt .$$

By letting $z = t - \tau$ it can be shown that $\bar{R}_V(-\tau) = \bar{R}_V(\tau)$, i.e. $\bar{R}_V(\tau)$ is an even function. It should be noted that

$$(2.11) \qquad \bar{R}_V(0) = \lim_{|T|\to\infty} \frac{1}{2T} \int_{-T}^{T} [V(t)]^2 dt ;$$

that is, $\bar{R}_V(0)$ is the mean square of V(t). In the absence of periodic or constant components of V(t),

$$(2.12) \qquad \lim_{|\tau|\to\infty} \bar{R}_V(\tau) = 0.$$ [1]

The power spectral density function or power spectrum is defined as the Fourier transform of the autocorrelation function:

---

[1] See Reference 2, p. 10.

$$(2.13) \qquad S_V(\omega) = \frac{1}{\sqrt{2\pi}} \int_{-\infty}^{\infty} \bar{R}_V(\tau)\, e^{-i\omega\tau} d\tau .$$

The power spectrum $S_V(\omega)$ associates a component of the mean square of $V(t)$ with every real value of the frequency ω.

The relation between an ergodic random function and its autocorrelation function is established as follows. (A random function, $W(t)$, defined over a finite range of t will be considered because, in practice, only finite records of random functions are encountered.) Let $W(t)$ represent a sample of an ergodic random process such that $W(t) = 0$ for $t < 0$ and for $t > T$. The Fourier transform of $W(t)$ is

$$(2.14) \qquad W_T(\omega) = \frac{1}{\sqrt{2\pi}} \int_{0}^{T} W(t)\, e^{-i\omega t} dt .$$

The power spectrum of $W(t)$ is then[2]

$$(2.15) \qquad S_W(\omega, T) = \frac{|W_T(\omega)|^2}{\sqrt{2\pi}\, T} .$$

$S_W(\omega, T)$ is a random variable that is a function of T and takes on different values for different members of its ensemble. In addition,

$$(2.16) \qquad \lim_{T \to \infty} \mathcal{E}[S_W(\omega, T)] = S_W(\omega)$$

---

[2] See Reference 2, p. 12

where $\mathcal{E}$ indicates expected value and the limit indicated is the same for all members of the ensemble. The autocorrelation function, as has been noted, is the Fourier transform of $S_w(\omega, T)$. Thus, if two ergodic random functions of finite duration are typical samples of the same ensemble, their autocorrelation functions will be the same within a small variation. Or, for such ergodic functions having the same probability density function, the more nearly coincident the autocorrelation functions, the higher the percent statistical confidence with which it may be said that the ergodic functions belong to the same ensemble.

2.3 Gaussian Random Number Generation

In the present study, the power residue method discussed in section (2.1), above, was programmed for use on an IBM 709 digital computer. For reference, that program is included in the Appendix, where it appears in the Subroutine for Uncorrelated Standard Normal Variable.

A statistical test to provide a measure of the uniformity of the distribution of the basic set was performed. Ideally, the elements of the basic set, denoted by B_i, should be distributed uniformly over a unit interval, indicating an equal probability of occurrence for each of the B_i. Accordingly, 1124 elements of the

basic set were generated and classified into 20 equal subintervals of the unit interval. The expected number of elements in each subinterval was, accordingly 1124 ÷ 20 = 56.2. Observed frequencies of occurrence, shown in Table 1, are clustered about the expected value. A quantitative measure of the uniformity of the distribution is given by the linear correlation coefficient, R_o, of the statistical frequencies shown in column 2 of Table 1. An $R_o = 0$ corresponds to a zero slope for the linear regression line and hence is associated with a uniform distribution. (R_o is defined as

$$R_o = \frac{\sum_{K=1}^{N} (Z_K - \bar{Z})\alpha_K}{\sum_{K=1}^{N} (Z_K - \bar{Z})^2}, \tag{2.17}$$

where Z_K = the number of the classification interval, α_K = the frequency of occurrence in the K^{th} interval, $\bar{Z}$ is the mean of the classification intervals, and N, in the present case, is 20.) The calculated value of R_o for the B_i was found to be -0.000983, indicating an apparently negligible slope for the regression line. This implies that the B_i are uniformly distributed to a very good approximation.

The elements, B_1, of the basic set were employed to construct a set of random numbers having a Gaussian

TABLE 1

DISTRIBUTION OF 1124 ELEMENTS OF THE "BASIC SET"

1	2	3	1	2	3
Z_K	α_K	Deviation from $Z = 56.2$	Z_K	α_K	Deviation from $Z = 56.2$
1	64	+ 7.8	11	53	- 3.2
2	63	+ 6.8	12	51	- 5.2
3	51	- 5.2	13	58	+ 1.8
4	64	+ 7.8	14	56	- 0.2
5	52	- 4.2	15	62	+ 5.8
6	54	- 2.2	16	66	+ 9.8
7	55	- 1.2	17	60	+ 3.8
8	46	-10.2	18	49	- 7.2
9	45	-11.2	19	59	+ 2.8
10	64	+ 7.8	20	52	- 4.2

probability density function, as follows. The probability density function of the B_i being

$$f(B) = \begin{cases} 1, & 0 \leq B \leq 1 \\ 0, & B < 0 \; ; \; B > 1, \end{cases} \tag{2.18}$$

the population mean, μ_B, and variance, σ_B^2, are

$$\mu_B = \int_0^1 B \, dB = \frac{1}{2}, \tag{2.19}$$

$$\sigma_B^2 = \int_0^1 (B - \tfrac{1}{2})^2 \, dB = \frac{1}{12}. \tag{2.20}$$

Let $\bar{B}_j$ denote elements of the set of sample means obtained from samples of size n taken from set B. That is,

$$\bar{B}_j = \frac{1}{n} \sum_{i=j}^{j+n} B_i, \qquad j = 1, n+2, 2n+3, \cdots. \tag{2.21}$$

By the central limit theorem of statistics,[3] the $\bar{B}_j$ have a probability density function that approaches a Gaussian distribution as $n \longrightarrow \infty$. Further, the mean, $\mu_{\bar{B}}$, of the population $\bar{B}$ is $\mu_B = \frac{1}{2}$ and the variance, $\sigma_{\bar{B}}^2$, is $\sigma_B^2/n = \frac{1}{12n}$. A compact expression for the previous statement is that the $\bar{B}_j$ are distributed as $N(\frac{1}{2}, \frac{1}{12n})$, indicating a normal (Gaussian) distribution with mean $\frac{1}{2}$ and

[3] See, for example, Reference 8, p. 107.

variance $\frac{1}{12n}$. It follows from the above that if a finite, but sufficiently large, n is chosen, the distribution of the $\bar{B}_j$ will approximate $N(\frac{1}{2},\frac{1}{12n})$.

The distribution of the $\bar{B}_j$ differs from that of an ideally Gaussian random variable in that the range of the former is (0,1) while the range of the latter is $(-\infty, +\infty)$. It is therefore necessary to choose n such that the variance $\sigma_{\bar{B}}^2$ is small enough to render the probability of occurrence of a $\bar{B}_j > 1$ or a $\bar{B}_j < 0$ negligible. The number of standard deviations $N_{\bar{B}}$ between $\mu_{\bar{B}}$ and the extreme values $\bar{B}_j = 0$, $\bar{B}_j = 1$ is

$$(2.22) \qquad N_{\bar{B}} = \frac{1 - \mu_{\bar{B}}}{\sigma_{\bar{B}}} = \frac{\mu_{\bar{B}} - 0}{\sigma_{\bar{B}}} = \frac{1}{2\sqrt{\frac{1}{12n}}} = \sqrt{3n} \ .$$

For $n = 25$, $N_{\bar{B}} = 8.66$. The probability of achieving a value of $\bar{B}_j$ more than 8.66 standard deviations from $\mu_{\bar{B}}$ is less than 0.00006. Therefore the possibility of achieving $\bar{B}_j > 1$ or $\bar{B}_j < 0$ was considered negligible; the value $n = 25$ was employed in the present investigation and was found to be satisfactory.

The above method of generating values of a Gaussian random variable by sampling from a uniformly distributed random variable was programmed for solution on a digital computer and appears, together with the power residue method, in the Appendix, where it appears in the Subroutine

for Uncorrelated Standard Normal Variable. Each entry into the subroutine of ENTRY STDNR causes 25 values of B_i (called LSTN in the program) to be generated by the power residue method. From those values, a $\bar{B}_j$ is computed by equation (2.21), above, and made available within the main program under the symbol XX.

2.4 Autocorrelated Random Function Simulation

From the set of numbers $\bar{B}$, a continuous, piecewise linear function, Q(t), is constructed as follows.

Pairs of Gaussian random numbers,

(2.23) $Q_i = \bar{B}_j$ and

(2.24) $T_i = \mu_T + \sigma_T \bar{B}_{j+1}$, $i = 1,2,\ldots q$, $j = 1,3,5,\ldots r$,

are defined in terms of the elements of set $\bar{B}$. Here, μ_T and σ_T are the preassigned mean and standard deviation of the T_i , which are interpreted as random increments of a continuous variable t . That is, $t_m = \sum_{i=1}^{m} T_i$, where t_m is a particular value of t . Corresponding to t_m is a value of Q(t) denoted by Q_m and determined from expression (2.23). By linearly interpolating between successive pairs $Q_1, t_1; \ldots; Q_q, t_q$, a continuous, piecewise linear function, Q(t), $0 \leq t \leq T$, is obtained. (Because a successful simulation was obtained with linear interpolation, no more complicated interpolating functions were

investigated.) A continuous, piecewise linear, random function, F(t), having a predetermined mean, $\bar{\mu}_F$, and variance, $\bar{\sigma}_F^2$, is obtained from Q(t) as follows. Let

$$F(t) = \begin{cases} \beta Q(t) + \alpha, & 0 \le t \le T \\ 0, & t < 0 \; ; \; t > T \end{cases} , \tag{2.25}$$

or

$$F_\ell = \beta Q_\ell + \alpha, \qquad \ell = 1, \cdots, n . \tag{2.26}$$

Then,

$$\bar{\mu}_F = \frac{1}{n} \sum_{\ell=1}^{n} F_\ell = \frac{1}{n} \sum_{\ell=1}^{n} [\beta Q_\ell + \alpha] = \beta \bar{\mu}_Q + \alpha , \tag{2.27}$$

$$\bar{\sigma}_F^2 = \frac{1}{n} \sum_{\ell=1}^{n} [F_\ell - \bar{\mu}_F]^2 = \beta^2 \bar{\sigma}_Q^2 . \tag{2.28}$$

Thus, $\beta = \bar{\sigma}_F / \bar{\sigma}_Q$ and $\alpha = \bar{\mu}_F - \beta \bar{\mu}_Q$, whence

$$F(t) = \frac{\bar{\sigma}_F}{\bar{\sigma}_Q} [Q(t) + \bar{\mu}_F - \bar{\mu}_Q] . \tag{2.29}$$

In the present investigation, $\bar{\mu}_F$ is chosen to be zero, whence

$$F(t) = \frac{\bar{\sigma}_F}{\bar{\sigma}_Q} [Q(t) - \bar{\mu}_Q] . \tag{2.30}$$

The computer program for constructing F(t) by the method outlined above appears in the Appendix as Segment 1 of the

main program. There, the interpolated values, F_ℓ, of F(t) are available for equal increments of time, δt, under the FORTRAN symbol FSMALL (I).

The percent statistical confidence with which it may be said that F(t) has a Gaussian probability density function was measured directly using a chi-square test. The quantity χ^2 is defined as

$$\chi^2 = \sum_{i=1}^{m} \frac{(o_i - e_i)^2}{e_i}, \tag{2.31}$$

where O_i is an "observed" value of a random variable, e_i is the "expected" value of that variable and m is the number of intervals into which the range of the random variable is, for convenience, divided. A value of $\chi^2 = 0$ indicates that $O_i = e_i$, $i = 1,\ldots,m$ and thus that the observed values may be said to have a Gaussian distribution with 100 per cent statistical confidence.

To test the statistical hypothesis that F(t), represented by the discrete interpolated values F_ℓ, has a Gaussian distribution, the population mean, μ_F, and variance, σ_F^2, of F(t) must be known; as predetermined measures of F(t), both μ_F and σ_F^2 are known quantities.

The range of t, i.e. $\bar{\mu}_F \pm 8.66\,\bar{\sigma}_F$, was divided into 23 intervals to provide a chi-square test with 23

statistical degrees of freedom. In any interval, i, bounded by values F_a and F_b $(a > b)$, the expected number of values of F_ℓ is

$$(2.32) \qquad e_i = n \int_{F_b}^{F_a} \phi(F)\, dF,$$

where n is the number of values of F_ℓ upon which χ^2 is to be based, and $\phi(F)$ is the Gaussian probability density function,

$$(2.33) \qquad \phi(F) = \frac{1}{\sqrt{2\pi}\,\sigma_F} \exp\left\{-\frac{(F-\mu_F)^2}{2\sigma_F^2}\right\}.$$

Integrals of the form given by expression (2.32) were approximated by summations

$$(2.34) \qquad e_i = n\,\Delta F \sum_{\ell=1}^{20} \phi_\ell \quad , \quad \Delta F = \frac{1}{20}\left[F_a - F_b\right],$$

and programmed for solution on a digital computer. That routine appears as Segment 2 of the program given in the Appendix. As a check on the accuracy of the numerical integration, a test quantity corresponding to

$$(2.35) \qquad \int_{-0.66\,\bar{\sigma}_F}^{0.66\,\bar{\sigma}_F} \phi(F)\, dF$$

was computed and given the symbol UNITY. (If the range of integration for integral (2.35) is extended to $(-\infty, +\infty)$, the value of that integral is unity in accordance with expression (2.3) of the definition for a probability density function.) The calculated value of UNITY was 1.000000 indicating an overall accuracy of at least seven significant figures.

The value of χ^2, as calculated from expression (2.31) and (2.32) based upon 5000 interpolated values F_ℓ, was found to be 3.496, which for 23 degrees of freedom implies that F(t) may be said to belong to a Gaussian distribution with better than 98 per cent statistical confidence.[4]

For a stationary F(t), the normalized autocorrelation function, $\bar{\bar{R}}_F$, is a function of τ only. (The autocorrelation function, expression (2.10), is normalized by dividing by the mean square, $\bar{R}_F(o)$.) That is, finite samples F(t), $0 \leq t \leq T$, will, for T sufficiently large, yield the same $\bar{\bar{R}}_F$ to a good approximation.

$\bar{\bar{R}}_F$ was calculated from the F_ℓ using numerical integration, based upon the series approximation

$$(2.36) \qquad \bar{\bar{R}}_F = \frac{\sum_{\ell=1}^{n} F_\ell F_{\ell+K}}{\sum_{\ell=1}^{n} F_\ell^2}, \qquad K = \tau/\delta t ,$$

[4] See Reference 8, Table III, p. 318.

as programmed in Segment 3 of the Appendix. The range, n, of ℓ is a measure of the averaging time, $T = n\,\delta t$. $\bar{\bar{R}}_F$ being an even function of τ, calculations were made only for non-negative values of τ. Functions $\bar{\bar{R}}_F$, for F(t), are shown in Figure 1, for averaging times ranging from 500 δt to 4500 δt. The curves of Figure 1 indicate that for averaging times $T \geq 1000\ \delta t$, $\bar{\bar{R}}_F$ behaves in a nearly stationary manner, the variations from the curve for $T = 1000\ \delta t$ being ≤ 0.03 in absolute value.

The particular value of δt to be chosen must be such that solutions of the equation of motion discussed below are numerically stable and convergent. In addition the time scale thus established should be consistent with a realistic $\bar{\bar{R}}_F$. Both criteria can be satisfied since $\delta t = \tau_1/n$ where δt is chosen to equal Δt (the finite increment of t for which solutions mentioned above are numerically stable and convergent), τ_1, is the value of τ at the first zero crossing of an empirically determined autocorrelation function, $\bar{\bar{R}}_E$, and n is the value of the abscissa at the first zero crossing in the curve for $T/\delta t = 1000$ in Figure 1. The value of n is in turn dependent upon ζ, the preassigned average number of F_ℓ's in an interval μ_r. (Although no rational functional relation between n and ζ is known to the author, it was found in practice that their magnitudes are very nearly

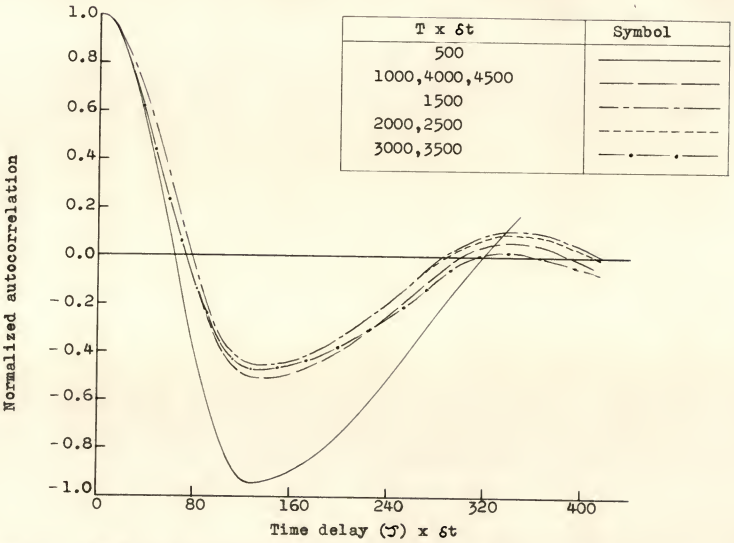

Fig. 1.--Normalized autocorrelation functions of F(t) for T/δt = 500,...,4500

equal for the values of n (or ζ) used in the present study.) The empirical autocorrelation function, $\bar{\bar{R}}_E(\tau)$, used is that recorded by Toubert, Kizner, and Nash (11,12). The works cited describe statistically the pressure signals obtained in the noise field of a turbulent subsonic air jet.

Figure 2 provides a comparison between $\bar{\bar{R}}_F(\tau)$ and the empirical autocorrelation function, $\bar{\bar{R}}_E(\tau)$, mentioned above. The curve $\bar{\bar{R}}_F(\tau)$ is there plotted with $n = 78$, from Figure 1 and hence $\delta t \simeq 0.6 \times 10^{-5}$ seconds; the effect is to cause $\bar{\bar{R}}_F$ to have the same first zero crossing point as $\bar{\bar{R}}_E$. The following should be noted: (1) $\bar{\bar{R}}_E$ and $\bar{\bar{R}}_F$ are indistinguishable for $|\tau| \leq 0.5$ milliseconds, (2) the absolute areal difference between the curves of $\bar{\bar{R}}_F$ and $\bar{\bar{R}}_E$ is 0.0784 milliseconds, i.e. 10.4 per cent of the gross area under the empirical curve, and (3) the form of $\bar{\bar{R}}_F$ conforms approximately to that of $\bar{\bar{R}}_E$. In the frequency domain, the power spectrum of $F(t)$ has an apparent upper bound at approximately 1300 cycles per second as does that for $F_E(t)$. The mean frequency for the bandwidth of $F(t)$ is 600 c.p.s. as compared with a mean frequency of 550 c.p.s. for the same bandwidth of $F_E(t)$.

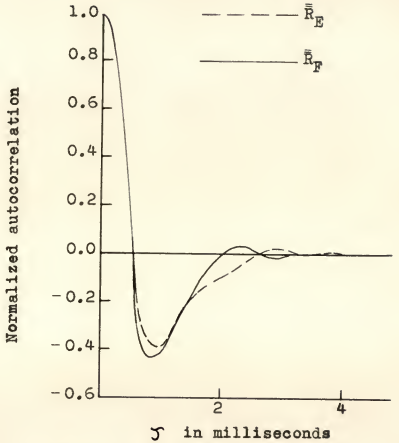

Fig. 2.--Comparison of autocorrelation functions $\bar{R}_E$ and $\bar{R}_F$

The function $F(t)$, generated by the method introduced in this chapter, was shown above to be (with better than 98% statistical confidence) a Gaussian random function. For averaging times $T \geq 1000\ \delta t$, $F(t)$ was shown to be stationary. The mean of $F(t)$ was predetermined to be zero. And $F(t)$ being continuous by definition, its autocorrelation function is also continuous. Thus, having satisfied the criteria noted in section (2.2), $F(t)$ has been shown to be ergodic. (Results obtained below by using $F(t)$ as a forcing function therefore apply to an entire class of random loads — that class having the same statistical properties as the sample $F(t)$.)

The empirical random function, $F_E(t)$, of which $\bar{\bar{R}}_E$ is the autocorrelation function, is also, to a good approximation, Gaussian and stationary, has a zero mean and continuous autocorrelation function, and hence is also ergodic (12). As is shown in Figure 2, $\bar{\bar{R}}_F$ closely approximates $\bar{\bar{R}}_E$, with $\delta t = 0.6 \times 10^{-5}$ seconds. F and F_E both being ergodic, and their autocorrelation functions differing only by small variations, the ensembles of which F and F_E, respectively, are members have similar statistical properties.

CHAPTER III

MATHEMATICAL MODEL OF THE BERNOULLI-EULER BEAM INCLUDING THE EFFECTS OF FINITE LATERAL DEFLECTION AND STRETCHING OF THE MIDDLE SURFACE

In linear beam theory, a Bernoulli-Euler beam is one in which the resistance to applied loads is assumed to arise from a bending couple proportionate to the curvature of the bent beam.[1] However, if the beam ends are restrained from translational displacements, the consequent equation of motion is exactly linear only for infinitesimal deflections. The nonlinearity of the equation, for finite deflections, arises from the presence of a term associated with the stretching of the middle surface of the beam. The assumptions underlying such a nonlinear Bernoulli-Euler beam model are presented in the following section. The beam model itself is a special case of the well known Von Karman plate equations (13).

3.1 Equation of Motion Under Transverse Load

The beam under consideration is referred to Lagrangian cartesian coordinates x,y,z. The middle surface of the beam is initially coincident with the x-z

[1] See Reference 13, pp. 2-3.

plane, the beam being oriented along the positive x axis. Motion is restricted such that displacements are parallel to the x-y plane.

Neglecting longitudinal inertia and damping, the differential equations of motion become

$$\frac{\partial \sigma_x}{\partial x} + \frac{\partial \sigma_{xy}}{\partial y} = 0, \tag{3.1}$$

$$\frac{\partial \sigma_y}{\partial y} dy\,dx - \sigma_x dy \frac{\partial w}{\partial x} + \left(\sigma_x + \frac{\partial \sigma_x}{\partial x} dx\right)\left(\frac{\partial w}{\partial x} + \frac{\partial^2 w}{\partial x^2} dx\right) dy + \frac{\partial \sigma_{xy}}{\partial x} dx\,dy + \frac{\partial \sigma_{yx}}{\partial y} dy\,dx \frac{\partial w}{\partial x} = \rho \frac{\partial^2 w}{\partial t^2} dx\,dy, \tag{3.2}$$

where w represents deflection in the y direction and ρ is mass per unit area parallel to the x-y plane.

Integrating equation (3.1) across the depth, h, of the beam yields

$$\frac{\partial}{\partial x}\int_{-\frac{h}{2}}^{\frac{h}{2}} \sigma_x dy + \sigma_{xy}\Big]_{-\frac{h}{2}}^{\frac{h}{2}} = 0. \tag{3.3}$$

Letting

$$N_x = \int_{-\frac{h}{2}}^{\frac{h}{2}} \sigma_x dy$$

and assuming zero shear stresses at the surfaces of the beam, equation (3.3) becomes

$$\frac{\partial}{\partial x} N_x = 0. \tag{3.4}$$

Thus, at any instant of time, N_x is constant throughout the length of the beam.

Equation (3.2) can be rewritten as

$$(3.5)\quad \frac{\partial \sigma_y}{\partial y} + \sigma_x \frac{\partial^2 w}{\partial x^2} + \frac{\partial \sigma_x}{\partial x}\frac{\partial w}{\partial x} + \frac{\partial \sigma_{xy}}{\partial x} + \frac{\partial \sigma_{xy}}{\partial y}\frac{\partial w}{\partial x} = \rho \frac{\partial^2 w}{\partial t^2},$$

where a term of order greater than two has been neglected. Integrating equation (3.5) across the depth of the beam yields

$$(3.6)\quad \sigma_y\Big|_{-\frac{h}{2}}^{\frac{h}{2}} + \frac{\partial^2 w}{\partial x^2} N_x + \frac{\partial}{\partial x} Q_x + \frac{\partial w}{\partial x}\left\{ \frac{\partial}{\partial x} N_x + \sigma_{yx}\Big|_{-\frac{h}{2}}^{\frac{h}{2}} \right\} = \rho h \frac{\partial^2 w}{\partial t^2},$$

where $Q_x = \int_{-\frac{h}{2}}^{\frac{h}{2}} \sigma_{xy}\, dy$.

Assuming

$$\sigma_y\Big|_{y=\frac{h}{2}} = q, \qquad \sigma_y\Big|_{y=-\frac{h}{2}} = 0,$$

where q represents a lateral surface load, and recalling that the term in braces is zero, equation (3.6) becomes

$$(3.7)\quad q + N_x \frac{\partial^2 w}{\partial x^2} + \frac{\partial}{\partial x} Q_x = \rho h \frac{\partial^2 w}{\partial t^2}.$$

Multiplying equation (3.1) by y and integrating over the depth of the beam yields

$$(3.8)\quad \frac{\partial}{\partial x} M_x + \left[y \sigma_{xy} \right]_{-\frac{h}{2}}^{\frac{h}{2}} - Q_x = 0,$$

$$(3.9)\quad \frac{\partial}{\partial x} M_x = Q_x,$$

where $M_x = \int_{-\frac{h}{2}}^{\frac{h}{2}} \sigma_x y \, dx.$

Noting from equation (3.9) that

$$(3.10)\quad \frac{\partial}{\partial x} Q_x = \frac{\partial^2 M_x}{\partial x^2}$$

and substituting equation (3.10) into equation (3.7) yields

$$(3.11)\quad q + N_x \frac{\partial^2 w}{\partial x^2} + \frac{\partial^2 M_x}{\partial x^2} = \rho h \frac{\partial^2 w}{\partial t^2}.$$

Quantities M_x and N_x can be expressed as functions of derivatives of deflection w. Assuming

$$(3.12)\quad \left(\frac{\partial w}{\partial x} \right)^2 \ll 1,$$

it follows that

$$(3.13)\quad \int_0^{L_1} ds - L \simeq \frac{N_x L}{AE}$$

where s is measured along the longitudinal axis of the

deformed beam, A is the cross-sectional area of the beam, E is Young's modulus, and L_1 is the length of the deformed longitudinal axis. Noting that

$$(3.14) \qquad ds = \sqrt{dx^2 + dw^2} = \sqrt{1 + \left(\frac{\partial w}{\partial x}\right)^2}\, dx,$$

it follows that

$$(3.15) \qquad ds = \left[1 + \frac{1}{2}\left(\frac{\partial w}{\partial x}\right)^2 - \frac{1}{8}\left(\frac{\partial w}{\partial x}\right)^4 + \cdots \right] dx,$$

$$(3.16) \qquad ds \simeq \left[1 + \frac{1}{2}\left(\frac{\partial w}{\partial x}\right)^2 \right] dx.$$

Substituting equation (3.16) into equation (3.13) yields

$$(3.17) \qquad N_x = \frac{AE}{2L} \int_0^L \left(\frac{\partial w}{\partial x}\right)^2 dx.$$

Let q consist of a forcing function $\mathcal{F}(x,t)$ and a linear damping term $K\frac{\partial w}{\partial t}$. Then, substituting equation (3.17) and the moment-curvature relation,

$$(3.18) \qquad M_x = -EI \frac{\partial^2 w}{\partial x^2},$$

into equation (3.11), the equation of motion is obtained in terms of deflection w:

$$(3.19)\qquad EI\frac{\partial^4 w}{\partial x^4} = -\rho A\frac{\partial^2 w}{\partial t^2} - K\frac{\partial w}{\partial t} + \mathcal{F}(x,t) + \frac{AE}{2L}\frac{\partial^2 w}{\partial x^2}\int_0^L\left(\frac{\partial w}{\partial x}\right)^2 dx,$$

where ρ is now considered to be mass per unit volume.

The difficulty of obtaining analytical solutions for the nonlinear integro-differential equation (3.19) is no obstacle to the numerical solution of that equation, assuming $\mathcal{F}(x,t)$ to be known. The following finite difference analogs are employed:

$$(3.20)\qquad w(x,t) \longrightarrow w_{i,j}$$

$$(3.21)\qquad \frac{\partial w}{\partial x} \longrightarrow \frac{w_{i+1,j} - w_{i-1,j}}{2(\Delta x)}$$

$$(3.22)\qquad \frac{\partial^2 w}{\partial x^2} \longrightarrow \frac{w_{i+1,j} - 2w_{i,j} + w_{i-1,j}}{(\Delta x)^2}$$

$$(3.23)\qquad \frac{\partial^4 w}{\partial x^4} \longrightarrow \left\{ w_{i+2,j} - 4w_{i+1,j} + 6w_{i,j} - 4w_{i-1,j} + w_{i-2,j} \right\} \div (\Delta x)^4,$$

$$(3.24)\qquad \frac{dw_i}{dt} \longrightarrow \frac{w_{i,j+1} - w_{i,j-1}}{2(\Delta t)},$$

where i and j correspond, respectively to the spatial coordinate, x, and time, t. Symbols Δx and Δt denote finite increments of x and t, each of which is

sufficiently small to assure convergence and stability of the numerical solution.

Substituting relations (3.20) through (3.23) into equation (3.19), and letting

$$(3.25) \qquad Y_{i,j} = \frac{dw_i}{dt} ,$$

results in the following equations of motion:

$$(3.26) \qquad \frac{dw_i}{dt} = Y_{i,j} \qquad \text{and}$$

$$(3.27) \qquad \frac{dY_i}{dt} = -\frac{EI}{\rho A(\Delta x)^4}\left[w_{i+2,j} - 4(w_{i+1,j} + w_{i-1,j}) + 6w_{i,j} - w_{i-2,j} \right] - \frac{K}{\rho A} Y_{i,j} + \frac{1}{\rho A} \tilde{f}_{i,j} + \frac{E}{8L\rho(\Delta x)^3} (w_{i+1,j} - 2w_{i,j} + w_{i-1,j}) \sum_{i=2}^{N} (w_{i+1,j} - w_{i-1,j})^2 ,$$

where stations $i = 2$ and $i = N$ define the locations of the beam ends $x = 0$ and $x = L$, respectively.

Substituting relation (3.24) and a similar one for Y_i into equations (3.26) and (3.27) yields

$$(3.28) \qquad w_{i,j+1} = 2(\Delta t) Y_{i,j} + w_{i,j-1} ,$$

$$(3.29)\quad Y_{i,j+1} = Y_{i,j-1} - \frac{2(\Delta t)K}{\rho A} Y_{ij} -$$

$$\frac{2(\Delta t)EI}{\rho A(\Delta x)^4}\left[w_{i+2,j} - 4(w_{i+1,j} + w_{i-1,j}) + \right.$$

$$\left. 6w_{ij} - w_{i-2,j} \right] + \frac{2(\Delta t)}{\rho A} \mathcal{F}_{ij} +$$

$$\frac{E(\Delta t)}{4L\rho(\Delta x)^3}(w_{i+1,j} - 2w_{ij} + w_{i-1,j}) \times$$

$$\sum_{i=2}^{N} (w_{i+1,j} - w_{i-1,j})^2.$$

Note that a separable solution has not been assumed. Together with boundary and initial conditions, equations (3.28) and (3.29) constitute an algorithm for determining $w(x,t)$ numerically.

3.2 Boundary and Initial Conditions

Physical boundary conditions may impose varying degrees of restraint against rotation and translation of the beam ends. The two limiting cases of rotational restraint, pinned and fixed ends, are considered in the present study. Similarly, the cases of no translational restraint and complete translational restraint at the ends are considered.

A pinned constraint, by definition, offers no resistance to rotation. The corresponding analytical boundary conditions are

$$w(a,t) = 0, \tag{3.30}$$

$$M_x(a,t) = 0, \tag{3.31}$$

where a denotes the value of x at a beam end. In view of equation (3.18), condition (3.31) may also be expressed as

$$\frac{\partial^2 w(a,t)}{\partial x^2} = 0. \tag{3.32}$$

In finite difference form, letting m denote an end station of the beam (m = 2,N), pinned boundary conditions (3.30) and (3.32) become

$$w_{m,j} = 0, \tag{3.33}$$

$$w_{m+1,j} = -w_{m-1,j}. \tag{3.34}$$

A fixed end constraint, by definition, permits no rotational motion of a beam end. The corresponding analytical boundary conditions are, therefore,

$$w(a,t) = 0, \tag{3.35}$$

$$\frac{\partial w(a,t)}{\partial x} = 0. \tag{3.36}$$

In finite difference form, fixed boundary conditions (3.35) and (3.36) become

(3.37) $w_{m,j} = 0,$

(3.38) $w_{m+1,j} = w_{m-1,j}.$

The initial conditions to be imposed are quite arbitrarily selected. The effect of initial conditions on the response of a damped beam will subside after a sufficiently great lapse of time. In the present study, statistical averages were taken over increasing averaging times until a stationary response was obtained. The simplest initial conditions, those of static equilibrium, were employed:

(3.39) $w(x,0) = 0,$

(3.40) $\frac{\partial w(x,0)}{\partial t} = 0.$

In finite difference form, initial conditions (3.39) and (3.40) become

(3.41) $w_{i,1} = 0$

(3.42) $w_{i,2} = w_{i,0},$

where $j = 1$ corresponds to $t = 0$.

The equations of motion (3.26) and (3.27), together with the boundary and initial conditions discussed in this section, were programmed for solution on a digital computer. The program appears as Segment 4 of the main program in the Appendix. The forcing function employed was a time-random concentrated load, P(t), located at midspan:

$$\mathcal{F}(x,t) = P(t)\,\delta(x - L/2), \tag{3.43}$$

where $$\delta(x - L/2) = \lim_{\epsilon \to 0} \begin{cases} 0, & x < (L-\epsilon)/2 \\ 1/\epsilon, & (L-\epsilon)/2 < x < (L+\epsilon)/2 \\ 0, & x > (L+\epsilon)/2 \end{cases}$$

and $P(t) = (\Delta x)F(t)$.

In finite difference terms,

$$\mathcal{F}_{i,j} = \begin{cases} F_j, & i = 1 + N/2 \\ 0, & i \neq 1 + N/2, \end{cases} \tag{3.44}$$

where $N = 6,10,14,18,\cdots$.

The range of N was chosen for convenience in determining the response at midspan and at the quarter points of the beam.

CHAPTER IV

DEFLECTION RESPONSE OF BEAMS TO DETERMINISTIC AND CORRELATED RANDOM FORCING FUNCTIONS

In solving a differential equation by numerical methods, criteria must be established for determining the stability and convergence of solutions. For all but the simplest equations, no general criteria are known.[1] In their absence, the most common technique used is to repeatedly reduce the magnitude of the finite increments until no appreciable change is observed in the response. That technique was employed in the present study.

4.1 Deflection Response for a Concentrated Load of Constant Magnitude Suddenly Applied at Midspan

To determine the range of values, for Δt and Δx, in which stable and convergent numerical solutions of equation (3.19) might be expected for a random forcing function, a preliminary study was made of a beam excited by a constant magnitude concentrated load applied suddenly at midspan. The end boundaries were assumed to be pinned and restrained against translational motion. Damping was

[1] See Reference 14, p. 489.

taken to be zero. The values of beam parameters used are listed in Table 2. They correspond to a rectangular steel beam of unit width, with a depth-to-length ratio of 1/20.

Many different values for s and x were employed in successive integrations of the equation of motion. It was found that numerical instability of the solution occurred for values of $\Delta t \geq 0.02$ milliseconds. The response was found to converge well for $\Delta x = L/16 = 2.5$ and $\Delta t \leq 0.006$ milliseconds.

Deflections at the midspan (x=L/2) and quarter points (X=L/4,3L/4) of the beam are shown in Figures 3 and 4 where P(t) was taken as

$$(4.1) \qquad P_1(t) = \begin{cases} 25^{\#}, & t \geq 0 \\ 0, & t < 0 \end{cases}$$

and

$$(4.2) \qquad P_2(t) = \begin{cases} 12{,}500^{\#}, & t \geq 0 \\ 0, & t < 0 \end{cases}$$

respectively. The magnitudes of P_1 and P_2 were chosen to obtain deflections well within the linear range of response for P_1 and well within the nonlinear range of response for P_2.

The curves of Figures 3 and 4 suggest a predominantly first mode response; w(L/2,t), w(L/4,t), and w(3L/4,t) are in phase and the deflection *vs.* time curves are sinusoidal

TABLE 2

NUMERICAL VALUES OF BEAM PARAMETERS

Symbol	Numerical Value (Units: in.-lb.-sec. system)
L	40
w	1
h	2
E	30×10^{6}
ρ	$.732 \times 10^{-3}$

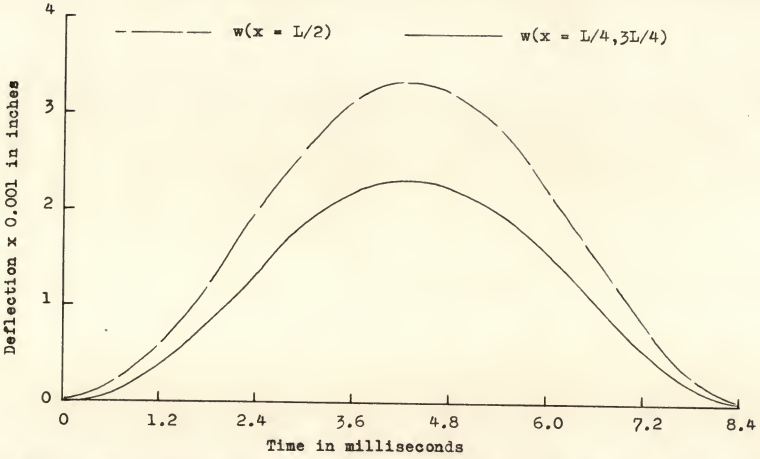

Fig. 3.--Deflection response for a concentrated load of 25 lb. applied suddenly at midspan

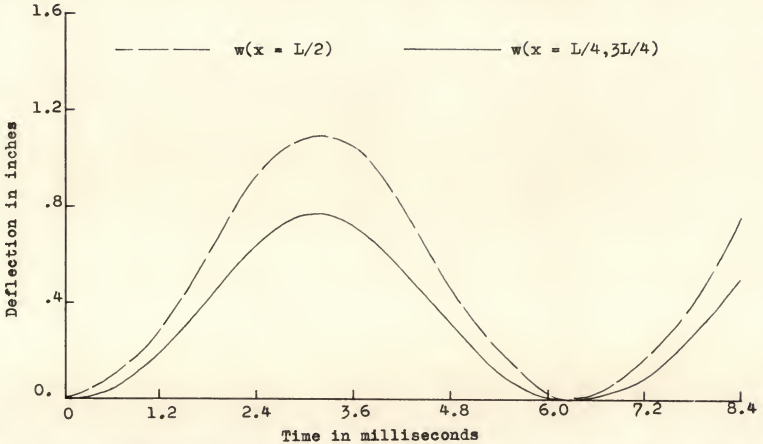

Fig. 4.--Nonlinear deflection response for a concentrated load of 12,500 lb. applied suddenly at midspan

in appearance. For purposes of comparison, the linear static deflections that would obtain at midspan under slowly applied concentrated loads of the same magnitude as the step functions, P_1 and P_2, were computed. Those calculated deflections were based upon an equivalent linear spring constant, K_E, defined as

$$(4.3) \quad K_E = \frac{P}{w} = \frac{48\,EI}{L^3} \; .$$

The amplitudes of the curves in Figure 3 indicate that the corresponding deflections can be anticipated to lie well within the linear range of response. (The maximum deflection-to-depth-of-beam vartio is 0.0017.) The double amplitude of w(L/2,t) should therefore be exactly twice the static deflection mentioned above. This expectation is in fact borne out: the double amplitude of w(L/2,t) is 0.3334×10^{-2} inches while the corresponding static deflection is $0.1666...\times 10^{-2}$ inches. Thus, with an accuracy of $(0.3334 \times 10^{-2} - 2 \times 0.1666...\times 10^{-2}) \div (0.333...\times 10^{-2}) = 0.021$ per cent, the double amplitude of w(L/2,t) equals twice the corresponding static deflection.

In Figure 4, the effects of restraining the beam ends against translation are observable. The frequency of the response has increased, as compared with the very nearly linear case shown in Figure 3. The linear static

deflection at midspan is, for Figure 4, approximately 0.83 inches. Thus, the double amplitude relative to the corresponding linear static deflection has been reduced as compared with the linear case illustrated in Figure 3. Stretching of the middle surface, caused by restraining the ends against translation, is sufficient to account for both the increase in frequency and relative decrease in amplitude.

4.2 Statistical Response to a Time-Random Concentrated Load Applied at Midspan

The equation of motion (3.19) in finite difference form (equations 3.28 and 3.29) was solved using the random load F(t) as a forcing function. Numerical solutions were carried out for several combinations of boundary conditions and preassigned values of σ_F^2. Values of beam parameters used are those listed in Table 2. In addition, the damping coefficient, K, was taken to be 0.5.

Samples of deflection responses, measured at midspan and at the quarter points of the beam, are shown for each of the cases studied in Figures 5 through 16. Response means and variances were computed under Segment 5 of the main program given in the Appendix. In no case was a response mean greater than 55 microinches obtained, indicating that all response means were found to be very nearly

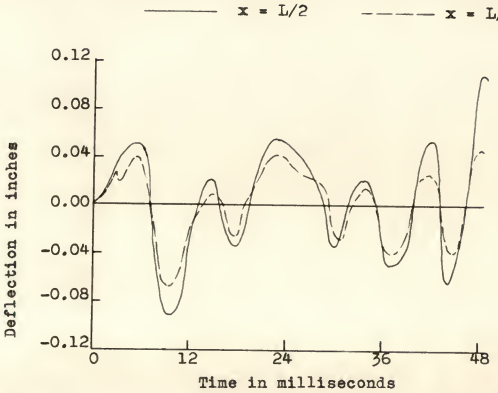

Fig. 5.--Nonlinear deflection response (σ_p = 1,000#, ends pinned)

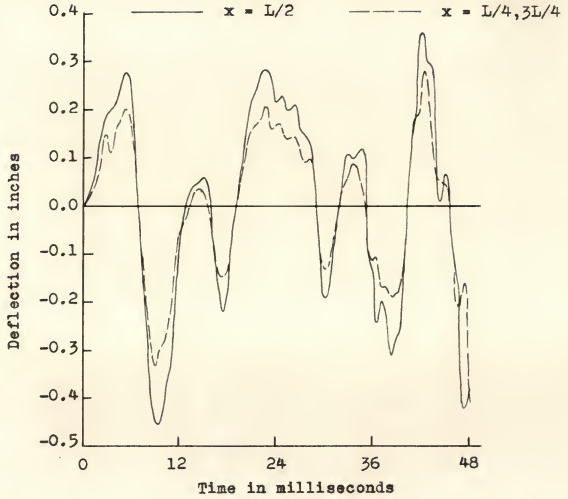

Fig. 6.--Nonlinear deflection response (σ_p = 5,000#, ends pinned)

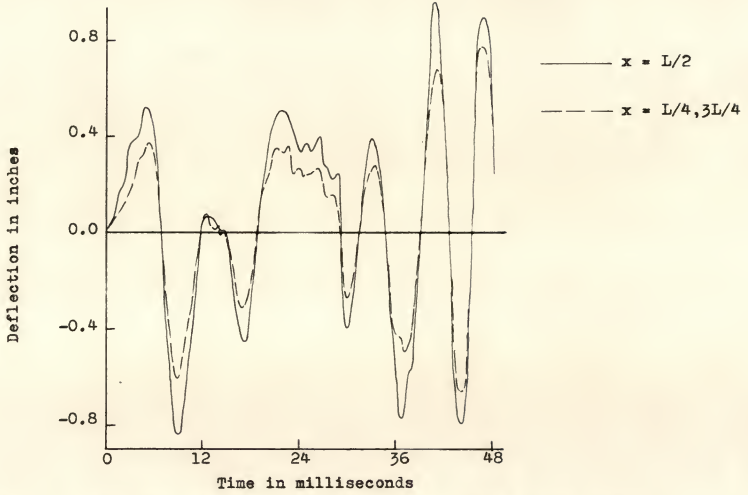

Fig. 7.--Nonlinear deflection response (σ_p = 10,000#, ends pinned)

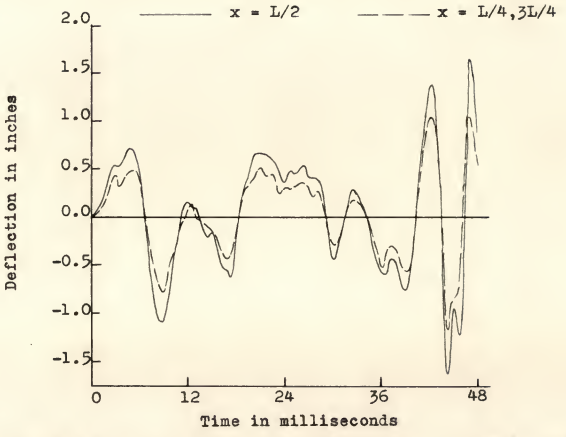

Fig. 8.--Nonlinear deflection response (σ_p = 15,000#, ends pinned)

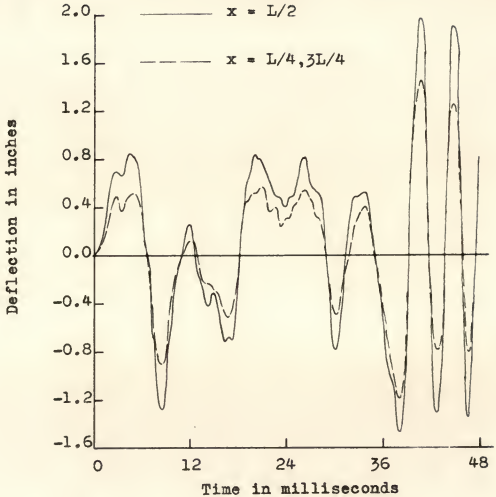

Fig. 9.--Nonlinear deflection response (σ_p = 20,000#, ends pinned)

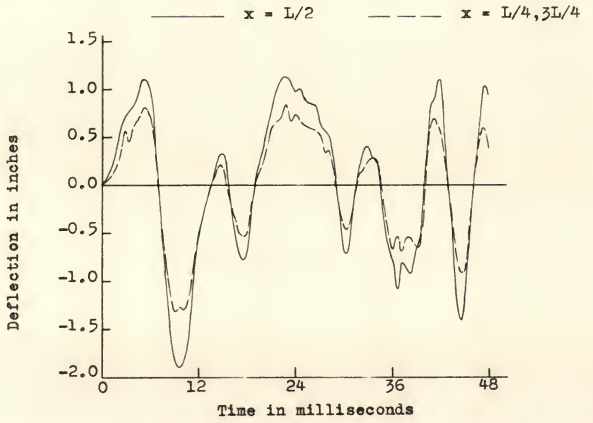

Fig. 10.--Linear deflection response (σ_p = 20,000#, ends pinned)

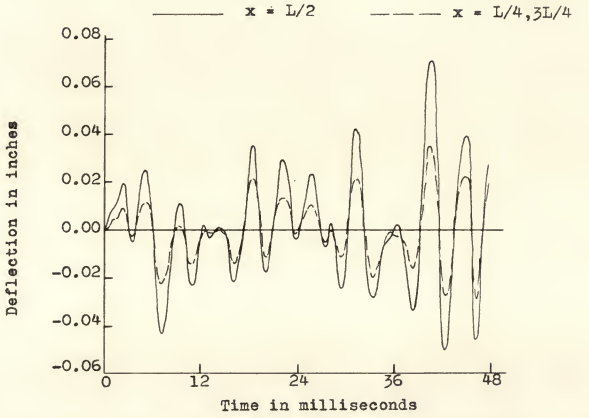

Fig. 11.--Nonlinear deflection response (σ_p = 1,000#, ends fixed)

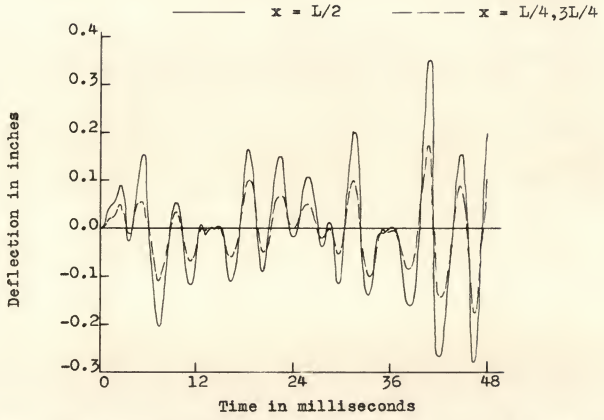

Fig. 12.--Nonlinear deflection response (σ_p = 5,000#, ends fixed)

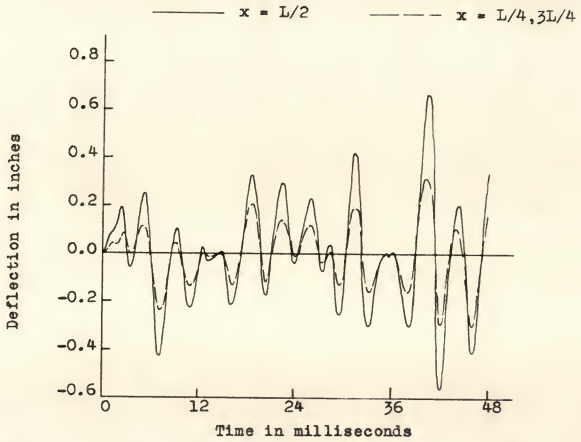

Fig. 13.--Nonlinear deflection response (σ_p = 10,000#, ends fixed)

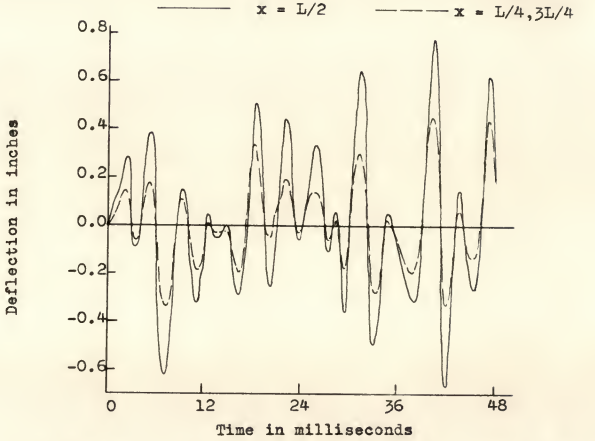

Fig. 14.--Nonlinear deflection response (σ_p = 15,000#, ends fixed)

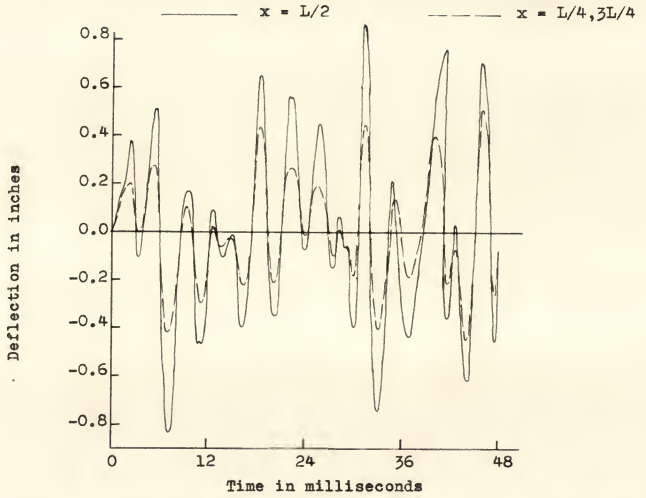

Fig. 15.--Nonlinear deflection response (σ_p = 20,000#, ends fixed)

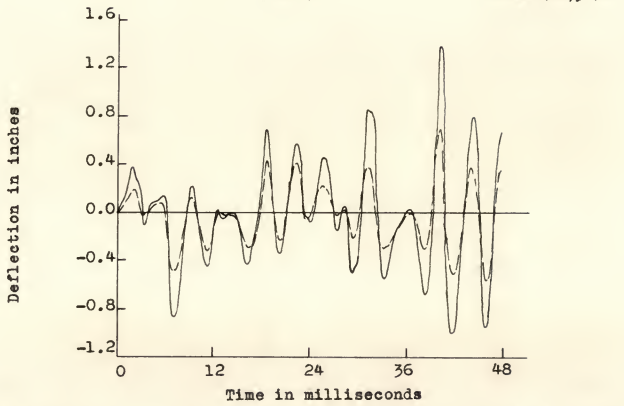

Fig. 16.--Linear deflection response (σ_p = 20,000#, ends fixed)

equal to zero. Response standard deviations are compared with the corresponding standard deviations of the excitation in Figures 17 and 18. Statistical frequency function approximations of the response probability density functions were obtained under the same segment of the main program and are shown for the linear cases and those nonlinear cases differing appreciably from the normal distribution in Figures 19 through 24.

Response autocorrelation functions and power spectra were computed under Segment 6 of the main program (see Appendix) and are shown, for the cases studied, in Figures 25 through 48. The autocorrelation functions are shown in normalized form to facilitate comparison. Corresponding power spectra shown are based upon the un-normalized autocorrelation functions.

Linear cases were established by introducing the constraint $N_x = 0$, which corresponds to beam ends unrestrained against longitudinal translation.

Numerical solutions of equations 3.28 and 3.29 were apparently convergent for $\Delta x \leq 2.5$ inches (L/16) and $\Delta t \leq 0.6 \times 10^{-5}$ seconds. Various averaging times were used in computing the response statistics. Stationary output was obtained in all cases for averaging times $T_1/\Delta t \geq 8000$.

The most salient feature of the deflection *vs.* time curves of Figures 5 through 16 is that in all cases,

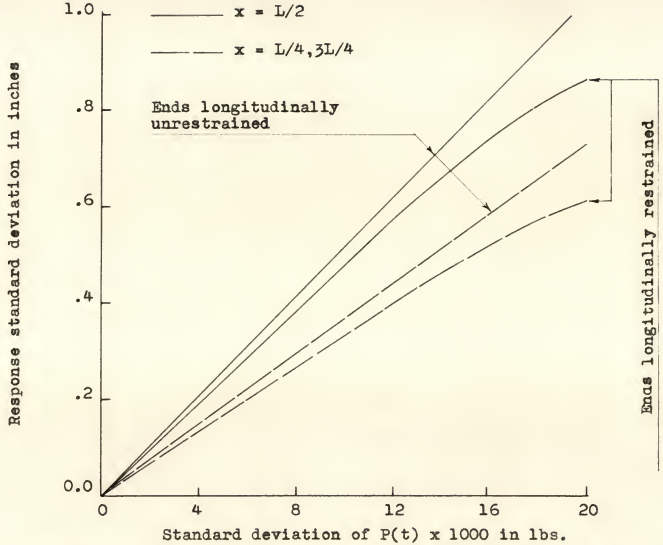

Fig. 17.--Excitation and response standard deviations (ends pinned)

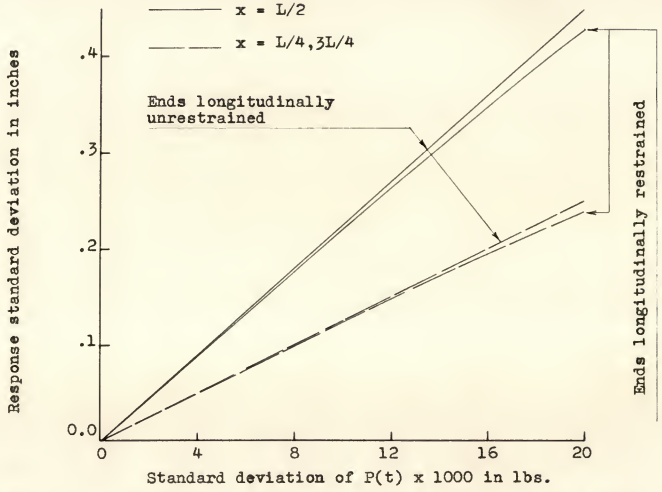

Fig. 18.--Excitation and response standard deviations (ends fixed)

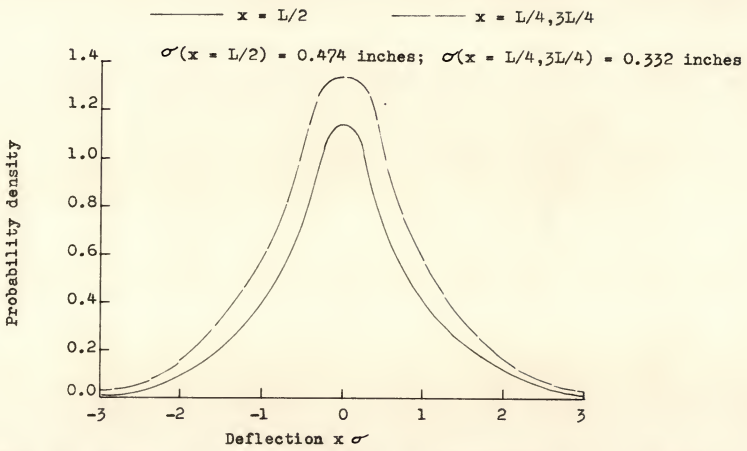

Fig. 19.--Nonlinear-response probability density functions (σ_p = 10,000#, ends pinned)

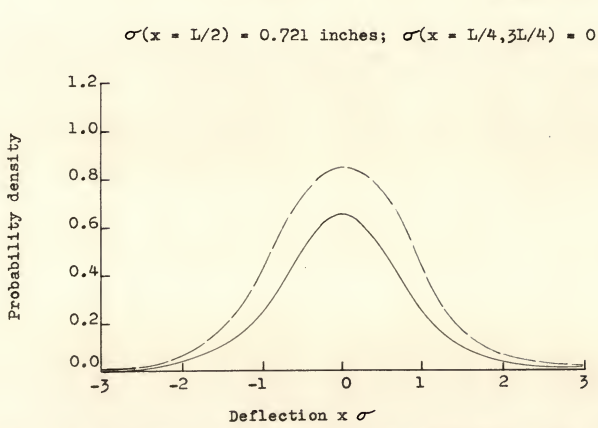

Fig. 20.--Nonlinear-response probability density functions (σ_p = 15,000#, ends pinned)

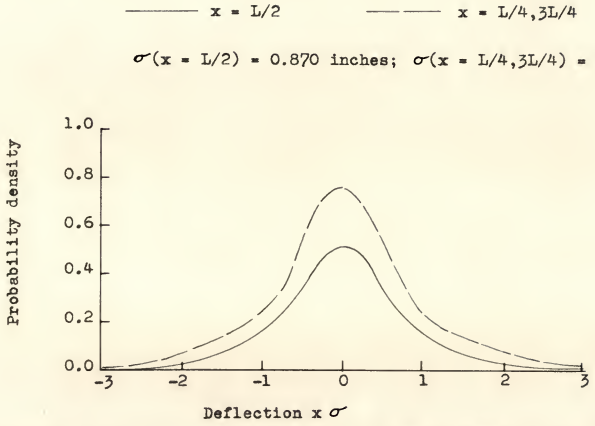

Fig. 21.--Nonlinear-response probability density functions (σ_p = 20,000#, ends pinned)

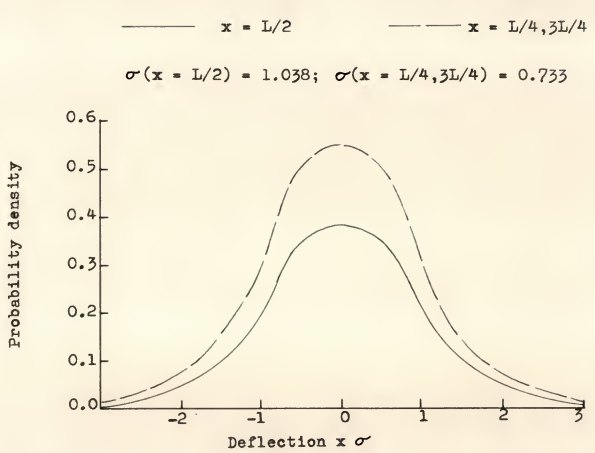

Fig. 22.--Linear-response probability density functions (σ_p = 20,000#, ends pinned)

———— x = L/2 —— —— x = L/4,3L/4

$\sigma(x = L/2) = 0.435$; $\sigma(x = L/4,3L/4) = 0.241$

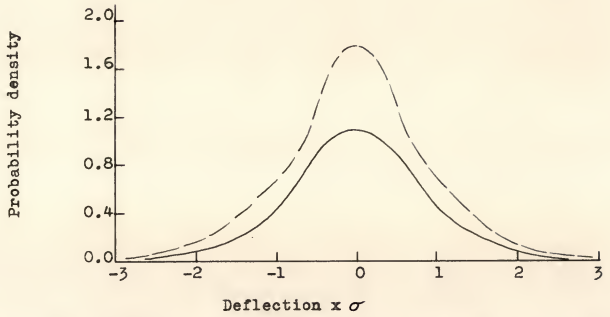

Fig. 23.--Nonlinear-response probability density functions (σ_p = 20,000#, ends fixed)

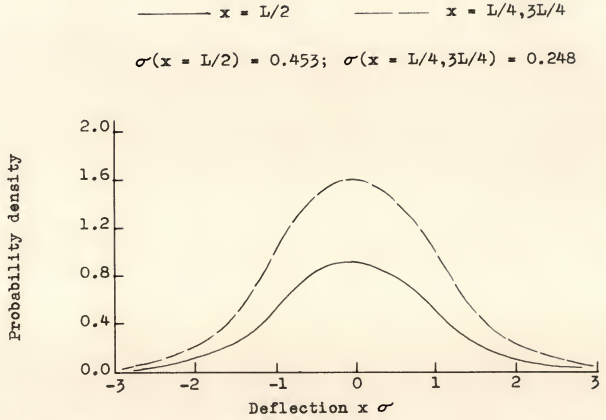

Fig. 24.--Linear-response probability density function (σ_p = 20,000#, ends fixed)

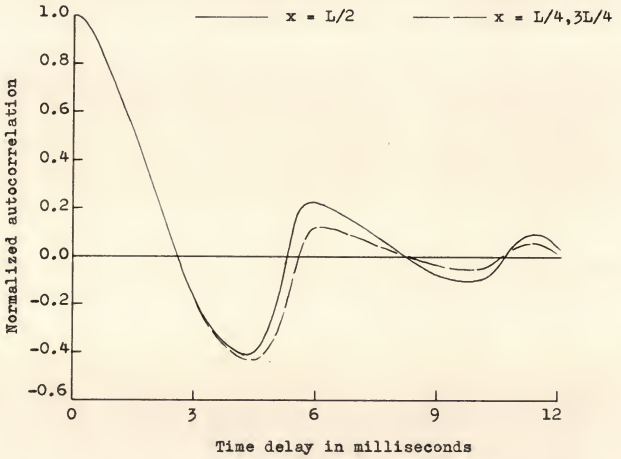

Fig. 25.--Nonlinear-response autocorrelation functions (σ_p = 1,000#, ends pinned)

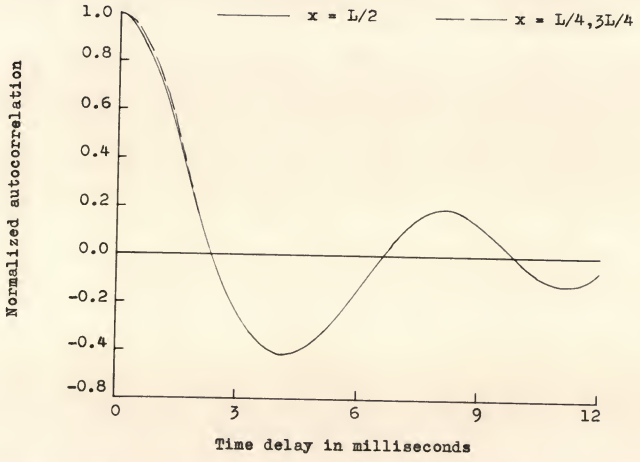

Fig. 26.--Nonlinear-response autocorrelation functions (σ_p = 5,000#, ends pinned)

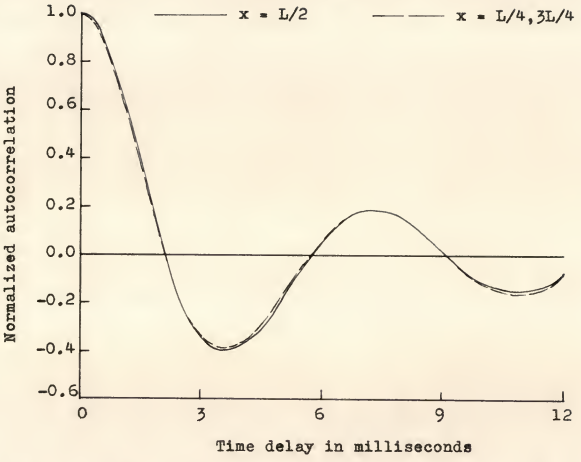

Fig. 27.--Nonlinear-response autocorrelation functions (σ_p = 10,000#, ends pinned)

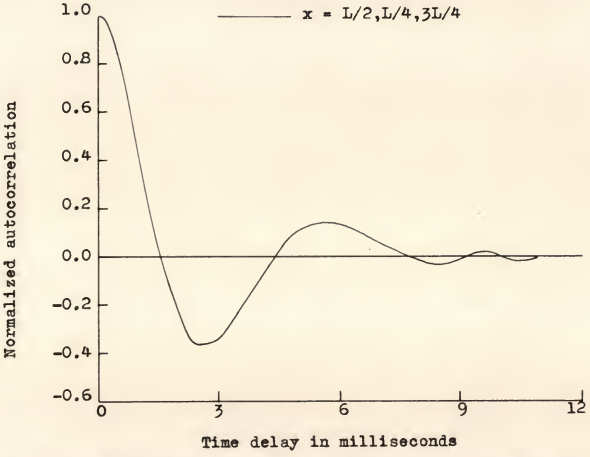

Fig. 28.--Nonlinear-response autocorrelation functions (σ_p = 15,000#, ends pinned)

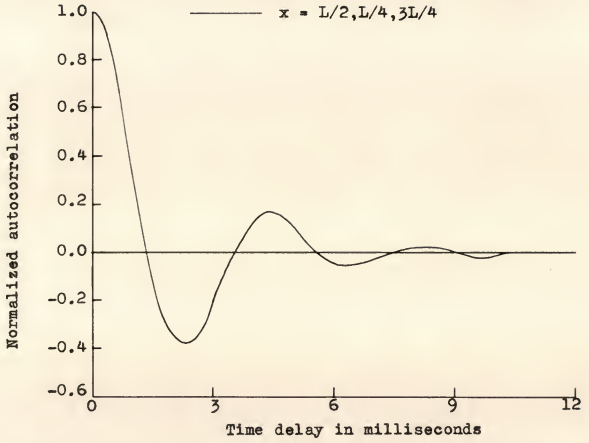

Fig. 29.--Nonlinear-response autocorrelation functions (σ_p = 20,000#, ends pinned)

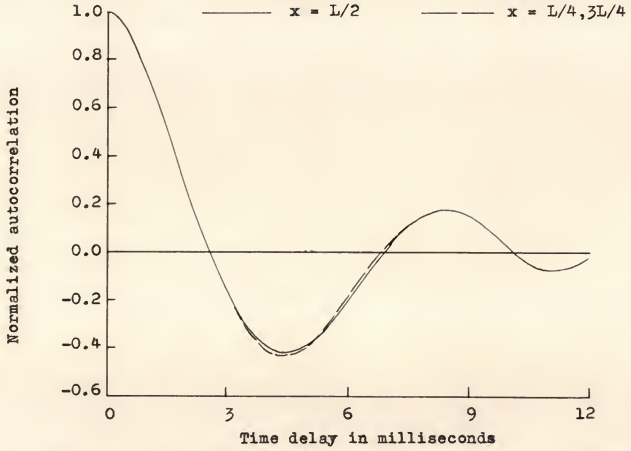

Fig. 30.--Linear-response autocorrelation functions (σ_p = 20,000#, ends pinned)

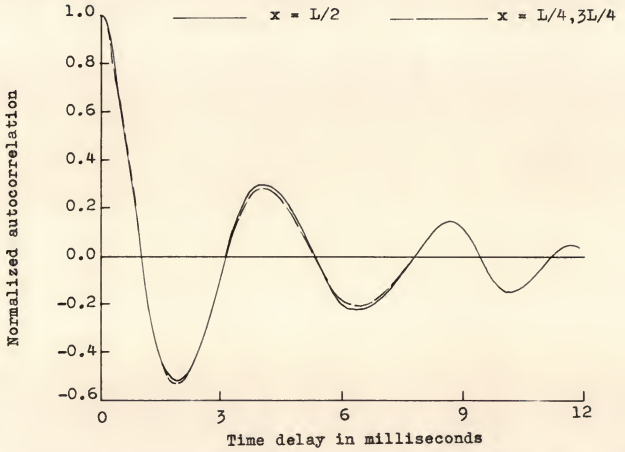

Fig. 31.--Nonlinear-response autocorrelation functions (σ_p = 1,000#, ends fixed)

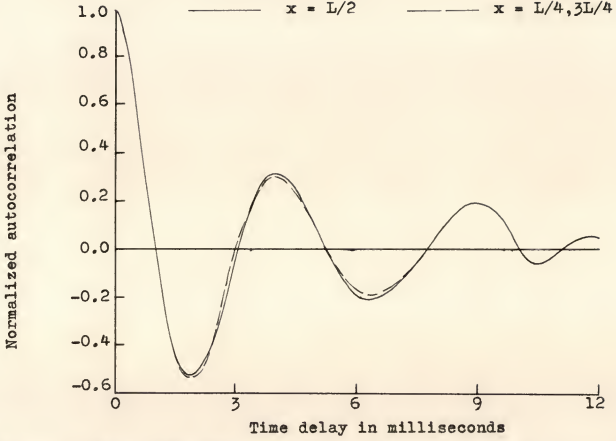

Fig. 32.--Nonlinear-response autocorrelation functions (σ_p = 5,000#, ends fixed)

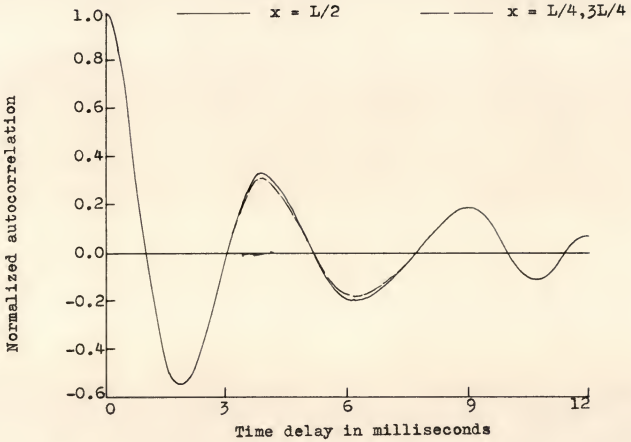

Fig. 33.--Nonlinear-response autocorrelation functions (σ_p = 10,000#, ends fixed)

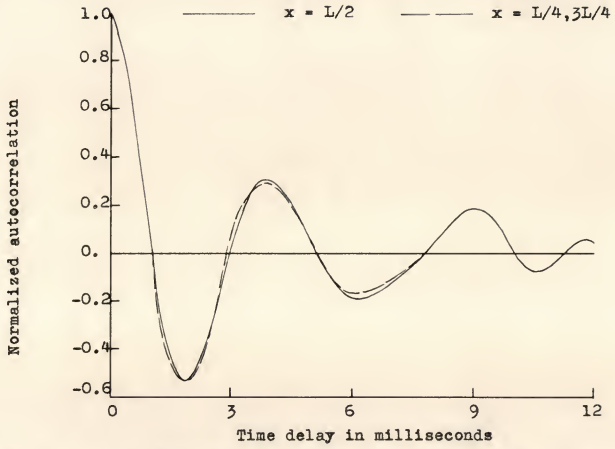

Fig. 34.--Nonlinear-response autocorrelation functions (σ_p = 15,000#, ends fixed)

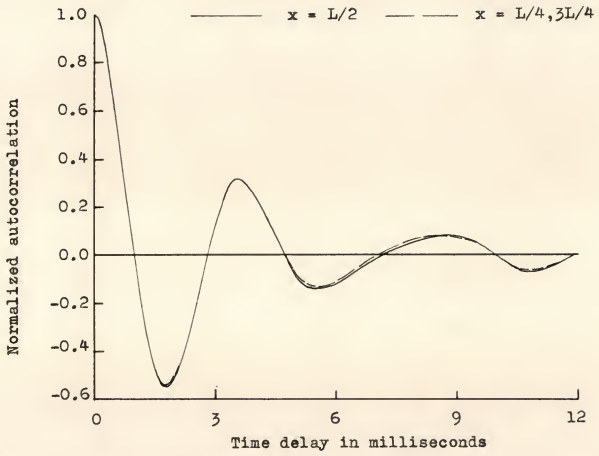

Fig. 35.--Nonlinear-response autocorrelation functions (σ_p = 20,000#, ends fixed)

Fig. 36.--Linear-response autocorrelation functions (σ_p = 20,000#, ends fixed)

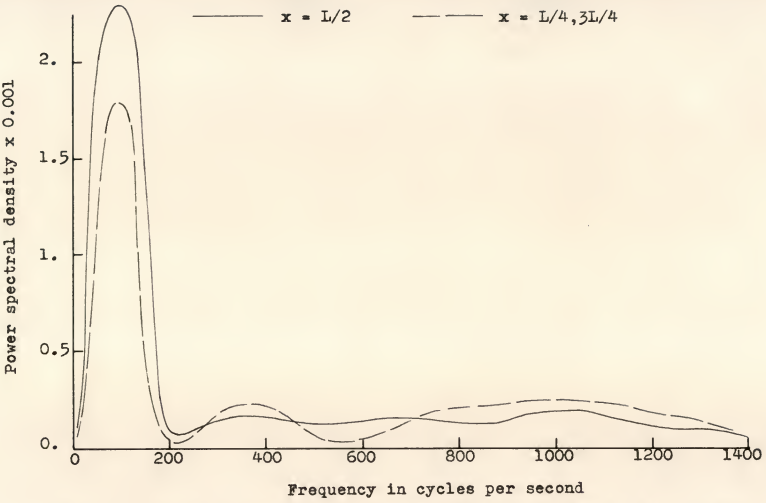

Fig. 37.--Nonlinear-response power spectra (σ_p = 1,000#, ends pinned)

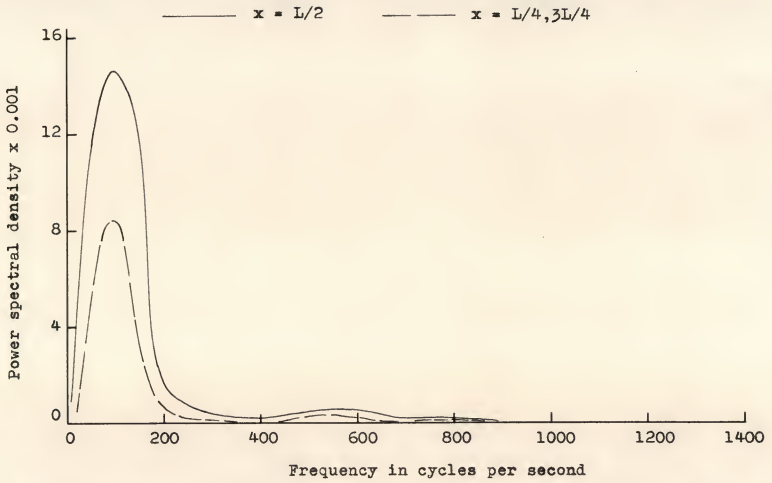

Fig. 38.--Nonlinear-response power spectra (σ_p = 5,000#, ends pinned)

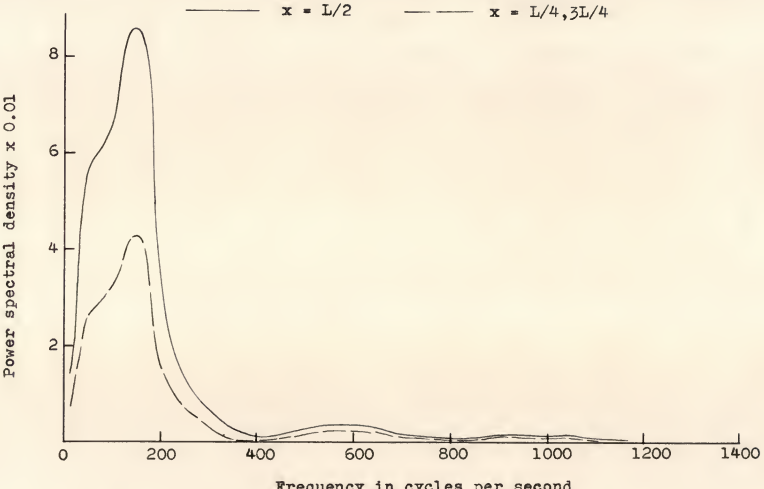

Fig. 39.--Nonlinear-response power spectra (σ_p = 10,000#, ends pinned)

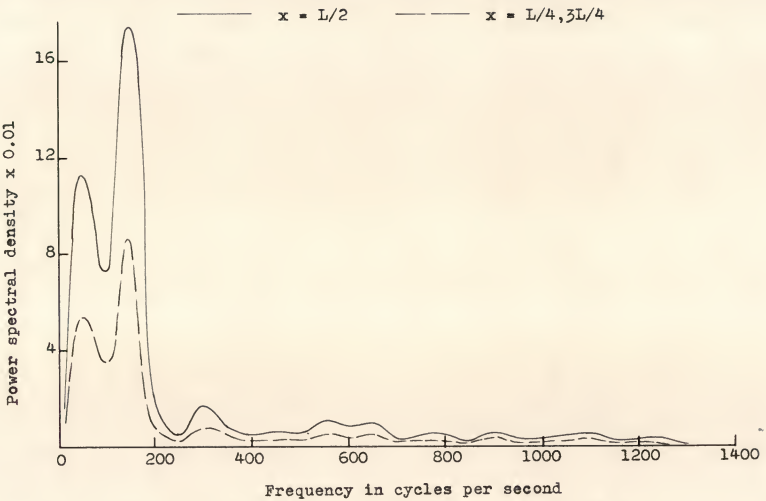

Fig. 40.--Nonlinear-response power spectra (σ_p = 15,000#, ends pinned)

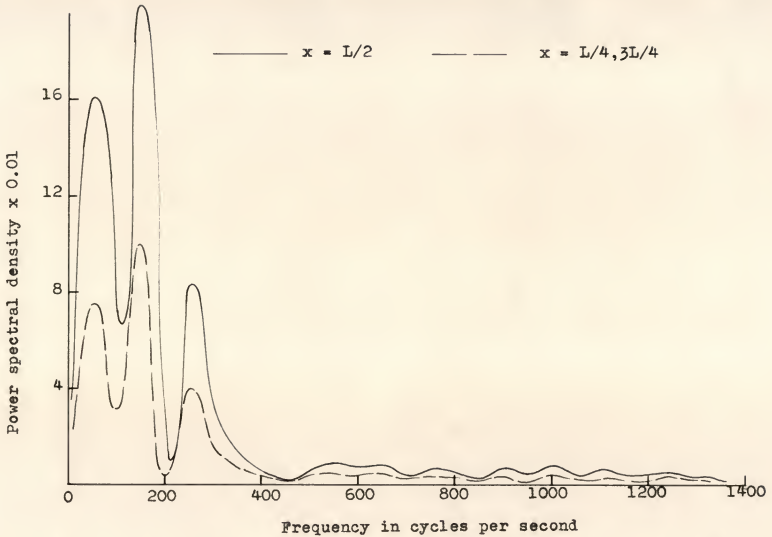

Fig. 41.--Nonlinear-response power spectra (σ_p = 20,000#, ends pinned)

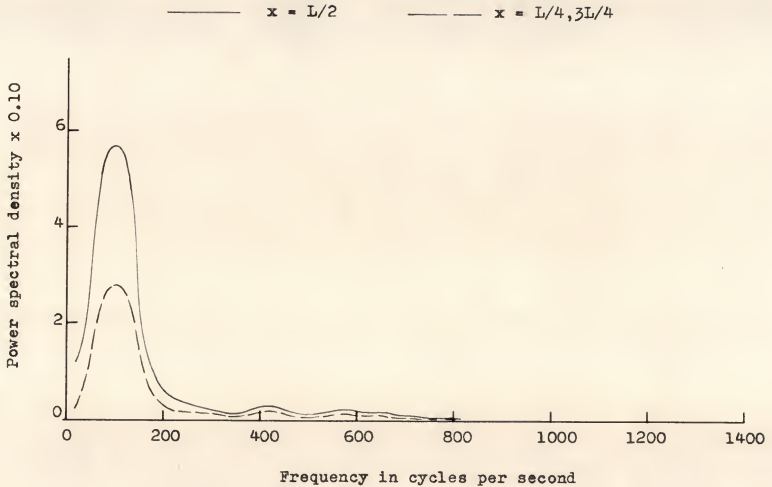

Fig. 42.--Linear-response power spectra (σ_p = 20,000#, ends pinned)

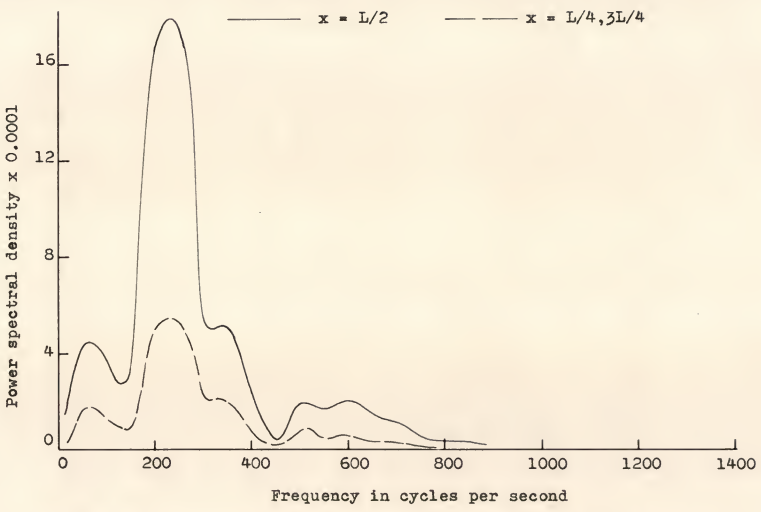

Fig. 43.--Nonlinear-response power spectra (σ_p = 1,000#, ends fixed)

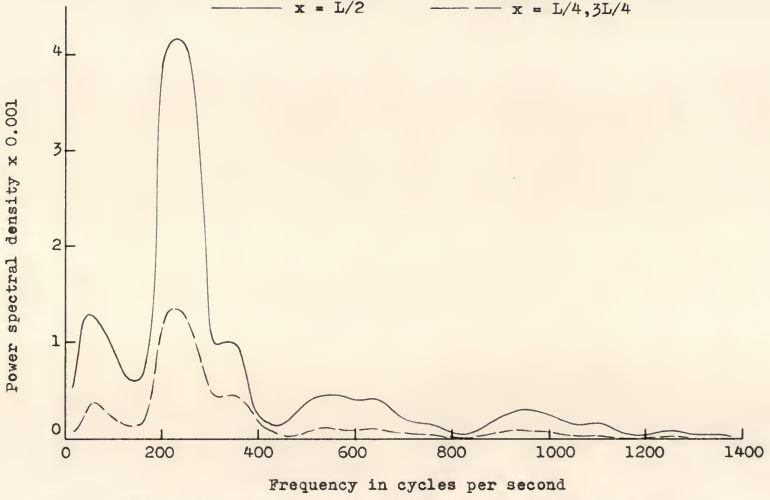

Fig. 44.--Nonlinear-response power spectra (σ_p = 5,000#, ends fixed)

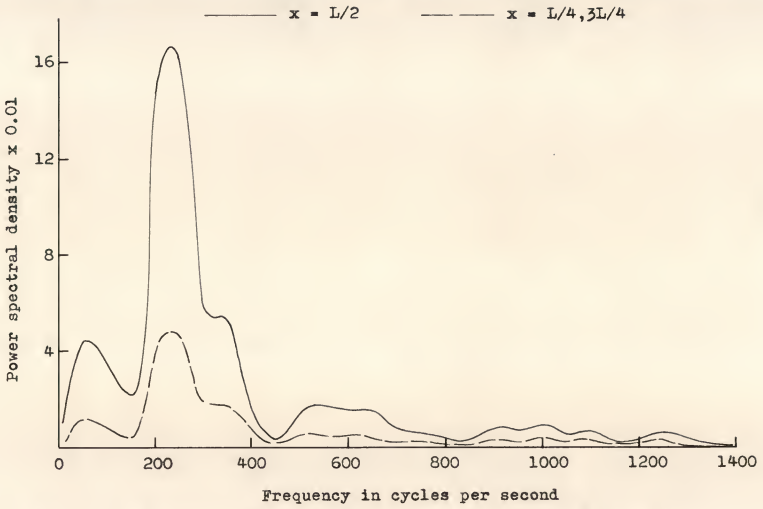

Fig. 45.--Nonlinear-response power spectra (σ_p = 10,000#, ends fixed)

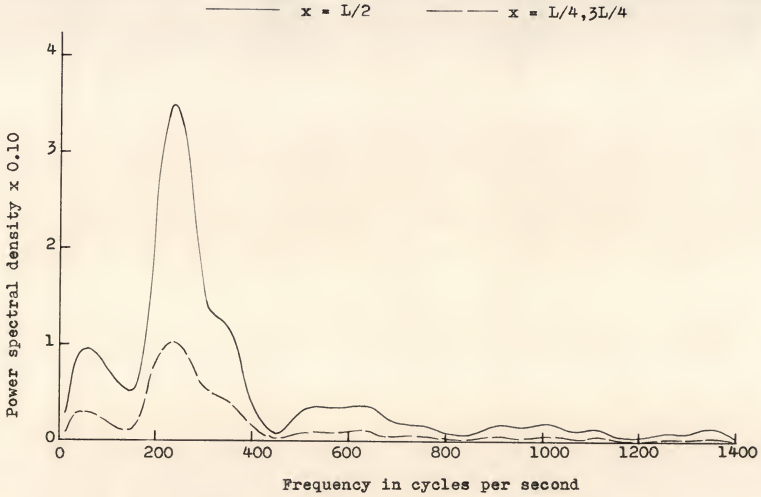

Fig. 46.--Nonlinear-response power spectra (σ_p = 15,000#, ends fixed)

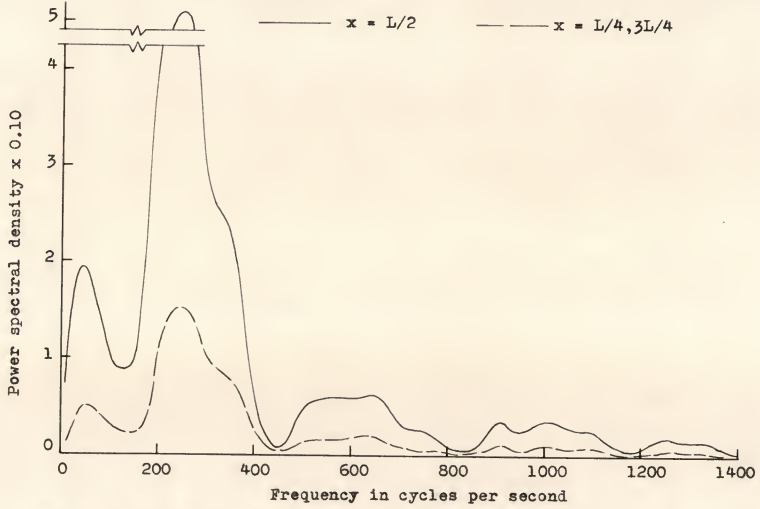

Fig. 47.--Nonlinear-response power spectra (σ_p = 20,000#, ends fixed)

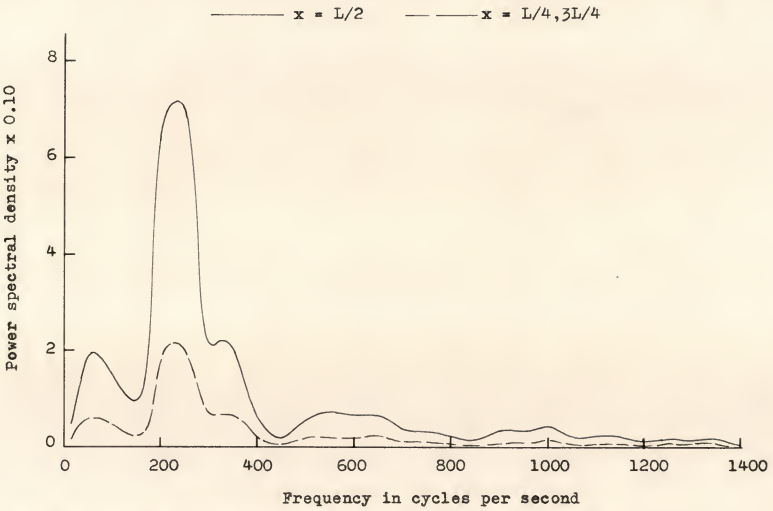

Fig. 48.--Linear-response power spectra (σ_p = 20,000#, ends fixed)

w(L/4,t), w(L/2,t), and w(3L/4,t) are "in phase" in the sense that w(L/4,t) and w(3L/4,t) correspond approximately to the deflection w(L/2,t) at a reduced ordinate scale. This feature of the curves is consistent with a predominantly first mode response. It is of interest to note that Herbert (5), in considering the response of a similar beam to uncorrelated (white noise) excitation, found that the first mode response was a good approximation to the total response, although higher modes contributed to the first mode itself (the modes being coupled in the nonlinear case). Figures 17 and 18 indicate that departures from linear response (ends unrestrained against longitudinal translation) are more significant for the more flexible pinned-end beam than for the stiffer rotationally fixed-end beam.

The nonlinear-response probability density functions (Figures 19 through 24) exhibit a characteristic increase in the probability density in the neighborhood of the mean deflection (w=0) and a corresponding decrease in the probability density for more extreme values, both effects being considered relative to a Gaussian distribution. This effect is consistent with the tendency of the stretched middle surface to restore the beam to equilibrium from any deformed position. The "distortion" of the probability density functions from the Gaussian form is not appreciable

for σ_p = 1,000#, 5,000# in the pinned end case and for σ_p = 1,000#, 5,000#, 10,000#, and 15,000# in the rotationally fixed-end case.

The response autocorrelation functions (Figures 25 through 36) exhibit the characteristic form that is described qualitatively as a variation of a damped cosine curve. Physical interpretations of these curves can be more easily visualized by considering them in the frequency domain, that is, by considering their corresponding power spectra (Figures 37 through 48).

The most salient feature of the power spectra is, in all cases, the presence of a single prominent peak. For increasing σ_p, two flanking peaks of considerably less magnitude emerge. The frequency responses shown indicate that the beam has, in effect, acted as a band pass filter with regard to the input power spectrum. The similarity in form of the response power spectra for x = L/2 and x = L/4,3L/4 and the prominent peak in each case is consistent with the predominantly first mode response affected by higher modes mentioned by Herbert (5).

CHAPTER V

CONCLUSIONS

The principal conclusions to be derived from the present study are as follows:

1) Using the method described in Chapter II, above, it is possible to generate a continuous, ergodic, random function whose statistical properties closely approximate those of pressure signals obtained experimentally from the noise field of a turbulent subsonic air jet.

2) Numerically stable and convergent solutions for the finite difference equivalents of the equation of motion of a beam, whose resistance to deformation is due to bending and stretching, can be obtained with numerical values of Δx and Δt large enough to render the use of existing digital computers practicable.

3) Solutions for a time-random concentrated load applied transversely at midspan contain strong indications that the total response is largely associated with the first mode, whose frequency varies with the contribution of higher modes in the nonlinear case.

4) For a given mean-square load, mean-square response was found to depart more from the linear response for the relatively flexible pinned-end beam than for the stiffer fixed-end beam.

Finally it should be noted that although the technique presented in this investigation was applied to a beam carrying a concentrated load, the method is in principle applicable to more complicated structural components and random load configurations.

APPENDIX

DIGITAL COMPUTER PROGRAM: 'SIMULATION;
RANDOM VIBRATIONS OF BEAMS'

```
    1  READ INPUT TAPE 5,301,FS,SMDT,NOD,LAP,NUMB,NT,NCELL
  301  FORMAT (2F7.0,2I5,3I3)
       READ INPUT TAPE 5,302,EL,WI,D,RHO,CEE,E,AA
  302  FORMAT (3F4.1,4F9.1)
       WRITE OUTPUT TAPE 6,303,FS,SMDT,NOD,LAP,NUMB,
     1 NT,NCELL,EL,WI,D,RHO,CEE,E,AA
  303  FORMAT (1H1/2E15.5,5I8///7E15.5)
       DIMENSION FSMALL (10000),BETA(23),GAMMA(23),
     1 GG(400),COR(400),PA(40),P(40),RA(40),R(40),QUAG(40),
     1 EA(40),Y(40),W(40),QA(2000),QB(2000),QC(2000),
     1 FF(2000),PRZ(50),PHI(1500)
c
c      SEGMENT 1. GENERATION OF RANDOM FORCING FUNCTION

       XX = 0.0
        T = 0.0
       TT = 0.0
       SFSM = 0.0
       SFSMS = 0.0
        I = 0
        H = SMDT
       CALL RESET
       DTMU = AA*SMDT
       SIGDT = 0.35*DTMU
       FPEAKA = 0.0
   10  CALL STDNR(XX)
       FPEAKB = XX
       NCHK = 0
   11  CALL STDNR(XX)
       DTPEAK = DTMU + SIGDT*XX
       IF(DTPEAK-SMDT)12,14,14
   12  NCHK = NCHK + 1
       IF (NCHK - 50)11,11,13
   13  WRITE OUTPUT TAPE 6,102
  102  FORMAT (1HO/1HO/30X20HEXECUTION TERMINATED///
     1 15X50H50 CONSECUTIVE VALUES OF DTPEAK ARE LESS
     1 THAN SMDT)
       GO TO 1
   14  SLOPE = (FPEAKB-FPEAKA)/DTPEAK
       I = I + 1
       FSMALL(I) = FPEAKA + SLOPE*(T-TT)
       TT = TT + DTPEAK
       GO TO 18
```

```
   15  T = T + SMDT
       IF (TT-T)16,16,17
   16  FPEAKA = FPEAKB
       GO TO 10
   17  JA = I
       I = I + 1
       FSMALL(I) = FSMALL(JA) + SLOPE*SMDT
   18  SFSM = SFSM + FSMALL(I)
       SFSMS = SFSMS + FSMALL(I)**2
       NFSM = NFSM + 1
       IF(NFSM-NOD)15,19,19
   19  TOTFSM = I
       FSMBAR = SFSM/TOTFSM
       FSMBSQ = FSMBAR**2
       SSUBFS = SFSMS/TOTFSM-FSMBSQ
   22  FSTDEV = SQRTF(SSUBFS)
       TQ = FS/FSTDEV
       DO 200 I = 1,NOD
  200  FSMALL(I) = TQ*(FSMALL(I)-FSMBAR)
C      END OF SEGMENT 1.
CCC
CCC    SEGMENT 2.  CHI SQUARE TEST TO DETERMINE THE
CCC    PER CENT STATISTICAL CONFIDENCE WITH WHICH THE
CCC    RANDOM FORCING FUNCTION MAY BE SAID TO BE GAUSSIAN.
       DDD = -8.66025*FS
       WW = 17.3205*FS/FLOATF(NCELL)
       WWW = WW/10.
       EEE = 2.*FS**2
       GGG = DDD
       BOT = DDD
       TOP = BOT + WW
       EPS = 0.
       DO25K = 1,NCELL
       ALPHA = 0.
   23  ALPHA = ALPHA + WWW/EXPF(GGG**2/EEE)
       GGG = GGG + WWW
       IF (GGG-TOP)23,24,24
   24  BETA(K) = FLOATF(NOD)*ALPHA*0.3989423/FS
       EPS = EPS + BETA(K)
       BOT = BOT + WW
   25  TOP = BOT + WW
       UNITY = EPS/FLOATF(NOD)
       DO36J = 1,NOD
       BOT = DDD
       TOP = BOT + WW
       DO35K = 1,NCELL
       IF (FSMALL(J)-BOT)34,32,31
   31  IF (TOP-FSMALL(J))34,32,33
   32  GAMMA(K) = GAMMA(K) + 0.5
       GO TO 36
```

```
   33  GAMMA(K) = GAMMA(K) + 1.0
       GO TO 36
   34  BOT = BOT + WW
   35  TOP = BOT + WW
   36  CONTINUE
       PAR = 0.
       DO38K = 1,NCELL
   38  PAR = PAR + (GAMMA(K)-BETA(K))**2/BETA(K)
       WRITE OUTPUT TAPE 6,106,PAR,UNITY
  106  FORMAT(1H1/1HO/25X,5HCH1SQ20X,5HUNITY/
     1 20X,F12.6,13X,F12.6///)
c      END OF SEGMENT 2.
c
c      SEGMENT 3.  AUTOCORRELATION FUNCTION
       DO39I = 1,NT
   39  GG(I) = 0.0
       JBB = NOD-NT
       LL = 1
       SQ = 0.0
       DO60L = LAP,JBB,LAP
       DO40J = LL,L
   40  SQ = SQ + FSMALL(J)**2
       DO50 I = 1,NT
       DO45J = LL,L
       K = I + J
   45  GG(I) = GG(I) + FSMALL(J)*FSMALL(K)
   50  COR(I) = GG(I)/SQ
       LL = L + 1
       WRITE OUTPUT TAPE 6,107,L
  107  FORMAT (1H1/1HO/20X,4HL = I4//14X,1HI23X,
     1 6HCOR(I)////)
       WRITE OUTPUT TAPE 6,108,(I,COR(I),I=1,NT)
  108  FORMAT(10X,I5,10X,E20.7)
   60  CONTINUE
c      END OF SEGMENT 3.
c
c      SEGMENT 4.  NUMERICAL INTEGRATION OF EQUATION
c      OF MOTION.
       MM = NUMB-2
       MB = 1
       MO = MM/4
       NALPHA = MO + 2
       NBETA = MM/2 + 2
       NGAMMA = NUMB-MO
       KEGA = NUMB + 1
       KEGB = NUMB - 1
       GO = MM
       DX = EL/GO
       A = WI*D
       BAR = (WI*D**3)/12.
```

```
      POE = 1./(RHO*A)
      CPOE = CEE*POE
      VA = E*BAR*POE/(DX**4)
      VB = VA*A*DX*0.125/(BAR*EL)
      HB = 2.*H
      DO300I = 1,KEGA
      PA(I) = 0.0
      P(I) = 0.0
      RA(I) = 0.0
  300 R(I) = 0.0
      DO500J = 1,NOD
      QUAG(NBETA) = FSMALL(J)
      ZIG = 0.0
      DO350I = 2,NUMB
      K = I + 1
      L = I - 1
  350 ZIG = ZIG + (P(K)-P(L))**2
      DO400I = 3,KEGB
      K = I + 1
      M = I + 2
      L = I - 1
      N = I - 2
      EA(I) = -CPOE*PA(I)-VA*(P(M)-4.*(P(K)+P(L))
     1 +6.*P(I)+P(N))+VB*(P(K)-2.*P(I)+P(L))*ZIG
     1 +POE*QUAG(I)
      Y(I) = RA(I)+HB*EA(I)
  400 W(I) = R(I)+HB*PA(I)
      W(KEGA) = W(KEGB)
      W(1) = W(3)
      Y(KEGA) = Y(KEGB)
      Y(1) = Y(3)
      MA = MA + 1
      IF (MA-5)415,410,410
  410 MA = 0
      QA(MB) = W(NALPHA)
      QB(MB) = W(NBETA)
      QC(MB) = W(NGAMMA)
      MB = MB + 1
  415 DO420I = 1,KEGA
      RA(I) = PA(I)
      R(I) = P(I)
      PA(I) = Y(I)
  420 P(I) = W(I)
  500 CONTINUE
      WRITE OUTPUT TAPE 6,501
  501 FORMAT(1H1/1HO/20X,9HW(NALPHA)10X,8HW(NBETA)
     1 12X,3HW(NGAMMA)///)
      WRITE OUTPUT TAPE 6,502,(QA(J),QB(J),QC(J),
     1 J = 20,MB,20)
  502 FORMAT(10X,3E20.5)
C     END OF SEGMENT 4.
```

```
C
C       SEGMENT 5.  MEAN,VARIANCE,AND PROBABILITY
C       DENSITY FUNCTION OF RESPONSE.
        DO510I = 1,MB
        RT = RT + QA(I)
        RS = RS + QB(I)
        RTZ = RTZ + QA(I)**2
  510   RSZ = RSZ + QB(I)**2
        FMB = MB
        QAMEAN = RT/FMB
        QBMEAN = RS/FMB
        QAUANC = RTZ/FMB - QAMEAN**2
        QBUANC = RSZ/FMB - QBMEAN**2
        WRITE OUTPUT TAPE 6,512,QAMEAN,QBMEAN,
       1 QAUANC,QBUANC
  512   FORMAT(1H1/1HO/33X,9HQAMEAN = E10.5,10X,
       1 9HQBMEAN = E10.5,//33X,9HQAUANC = E10.5,10X,
       1 9HQBUANC = E10.5////)
        DO550J = 1,MB

  550   FF(J) = QA(J)
        FMN = QAMEAN
        FU = QAUANC
        WW = 0.12*SQRTF(FU)
        DDD = FMN-3.*SQRTF(FU)
        GO TO 600
  552   DO551I = 1,50
  551   PRZ(I) = 0.0
        DO555J = 1,MB
  555   FF(J) = QB(J)
        FMN = QBMEAN
        FU = QBUANC
        WW = 0.12*SQRTF(FU)
        DDD = FMN-3.*SQRTF(FU)
  600   DO650J = 1,MB
        BOT = DDD
        TOP = BOT + WW
        DO635K = 1,50
        IF(FF(J)-BOT)634,632,631
  631   IF(TOP-FF(J))634,632,633
  632   PRZ(K) = PRZ(K) + 0.5
        GO TO 650
  633   PRZ(K) = PRZ(K) + 1.0
        GO TO 650
  634   BOT = BOT + WW
  635   TOP = BOT + WW
  650   CONTINUE
        DO 620K = 1,50
  620   PRZ(K) = PRZ(K)/(FMB*WW)
        IR = IR + 1
        IF(IR-2)660,670,670
```

```
      660  WRITE OUTPUT TAPE 6,700
      700  FORMAT(40X,41HPROBABILITY DENSITY FUNCTION
     1 OF W(NALPHA)////)
           WRITE OUTPUT TAPE 6,701,(I,PRZ(I),I = 1,50)
      701  FORMAT(40X,I2,E20.5)
           GO TO 552
      670  WRITE OUTPUT TAPE 6,702
      702  FORMAT(1H1/1HO/40X,40HPROBABILITY DENSITY
     1 FUNCTION OF W(NBETA)///)
           WRITE OUTPUT TAPE 6,701,(I,PRZ(I),I=1,50)
c          END OF SEGMENT 5.
c
c
c          SEGMENT 6. RESPONSE AUTOCORRELATION FUNCTIONS
c          AND POWER SPECTRA.
           DO750I = 1,MB
      750  FF(I) = QA(I)
           GO TO 800
      755  DO 760I = 1,MB
      760  FF(I) = QB(I)
      800  DO 839I = 1,NT
           COR(I) = 0.0
      839  GG(I) = 0.0
           JBB = MB-NT
           LL = 1
           SQ = 0.0
           MBS = MB/10
           MBA = 9*MBS
           DO860L = MBA,MB,MBS
           DO840J = LL,L
      840  SQ = SQ + FF(J)**2
           DO850I = 1,NT
           DO845J = LL,L
           K = I + J
      845  GG(I) = GG(I) + FF(J)*FF(K)
      850  COR(I) = GG(I)/SQ
           LL = L + 1
           WRITE OUTPUT TAPE 6,900,L
      900  FORMAT(1H1/1HO/20X,11HOUTPUTL = I4//14X,
     1 1HI23X,6HCOR(I)////)
           WRITE OUTPUT TAPE 6,908,(I,COR(I),I=10,NT,10)
      908  FORMAT(10X,I5,10X,E20.7)
           DO841I = 1,NT
      841  COR(I) = GG(I)
           DTAU = 5.*SMDT
           DOUB = 2.*DTAU
           DARG = 6.28318*DTAU
           DO855I = 50,1500,50
           SLAM = 0.0
           DO854K = 1,NT
```

```
    854  SLAM = SLAM + COR(K)*COSF(FLOATF(I*K)*DARG)
    855  PH1(I) = DOUB*(0.5+SLAM)
         WRITE OUTPUT TAPE 6,910
    910  FORMAT(///10X,39HSPECTRALDENSITYCORRESPONDING
        1 TO ABOVE/10X,24HAUTOCORRELATION FUNCTION//)
         WRITE OUTPUT TAPE 6,911
    911  FORMAT(14X,1HJ23X,6HPHI(J)//)
         WRITE OUTPUT TAPE 6,908,(I,PHI(I),I=50,1500,50)
    860  CONTINUE
         NCOB = NCOB + 1
         IF(NCOB-2)755,870,870
    870  WRITE OUTPUT TAPE 6,909
    909  FORMAT(//10X,41HEND OF RESPONSE
        1 AUTOCORRELATION FUNCTIONS)
c        END OF SEGMENT 6.
         CALL EXIT
         END
*        FAP
         SUBROUTINE FOR UNCORRELATED STANDARD NORMAL VARIABLE
         ENTRY STDNR
         ENTRY RESET
 STDNR   SXA XR,1
         STZ SUM
         AXT 25,1
1)       LDQ GEN
         MPY LSTN
         STQ LSTN
         CLA LSTN
         ARS 8
         ORA CONS
         FSB CONS
         ACL -1B8
         FAD SUM
         STO SUM
         TIX 1),1,1
         CLA SUM
         FDH = 25.
         XCA
         FSB CONS
         XCA
         FMP = 17.3205
         STO* 1,4
    XR   AXT **,1
         TRA 2,4
 RESET   CLA SET
         STO LSTN
         TRA 1,4
   GEN   DEC 1220703125
  CONS   DEC 0.5
 LSTN    BCI 1,C00001
   SET   BCI 1,C00001
   SUM
         END
```

LIST OF REFERENCES

1. Crandall, Stephen H., Editor. Random Vibration. The Technology Press, Cambridge, Mass., 1958.

2. Crandall, Stephen H., Editor. Random Vibration, Volume II. The Technology Press, Cambridge, Mass., 1963.

3. Smith, P. W., Jr. "Response of Nonlinear Structures to Random Excitation." Journal of the Acoustical Society of America, Vol. 34, New York, 1962.

4. Andronov, A. A., Pontryagin, L. S., and Vitt, A. A. "On the Statistical Investigation of Dynamical Systems." Journal of Experimental and Theoretical Physics, Vol. 3, 1933.

5. Herbert, Richard E. Random Vibrations of Nonlinear Systems. Doctoral dissertation. University of Florida, Gainesville, Florida, 1964.

6. Milne, W. E. Numerical Calculus. Princeton University Press, Princeton, N. J., 1949.

7. Kahn, H. Applications of Monte Carlo. Research Memorandum 1237-AEC, The Rand Corporation, Santa Monica, Calif., 19 April, 1954, revised 27 April, 1956.

8. Hoel, P. G. Introduction to Mathematical Statistics. John Wiley & Sons, Inc., New York, 1954.

9. Taussky, O. and Todd, J. "Generation of Pseudo-Random Numbers." In Meyer, H.A., Ed. Symposium on Monte Carlo Methods. John Wiley & Sons, Inc., New York, 1954.

10. International Business Machines Corporation. Random Number Generation and Testing. New York, 1959.

11. Trubert, M. R. P., Kizner, G. H., and Nash, W. A. Experimental Determination of a Statistical Representation of the Noise Field of a Subsonic Air Jet. Air Force Office of Scientific Research Technical Note 61-991 (unclassified), August, 1961.

12. Kizner, G. H. Experimental Determination of Transfer Functions of Beams and Plates by Cross-Correlation Techniques. Doctoral Dissertation, University of Florida, Gainesville, Florida, June, 1962.

13. Love, A.E.H. A Treatise on the Mathematical Theory of Elasticity, 4th Edition. Dover Publications, New York, 1927.

14. Beckenbach, Edwin F. Modern Mathematics for the Engineer. McGraw-Hill Book Company, Inc., New York, 1956.

BIOGRAPHICAL SKETCH

Donald Joseph Belz was born September 5, 1938, in the City of New York, New York. In June, 1956, he was graduated from the Brooklyn Technical High School. In June, 1960, he received the degree Bachelor of Civil Engineering from the Cooper Union. The following September he enrolled in the Graduate School of the University of Florida. He taught as an Interim Instructor in the Department of Engineering Mechanics until January, 1962, when he received the degree Master of Science in Engineering. From February, 1962, through August, 1962, he held the position of Research Engineer at the Franklin Institute in Philadelphia, Pennsylvania. In September, 1962, he resumed his graduate studies at the University of Florida. During the academic year 1962-1963 and again in 1963-1964 he held the position of Graduate Fellow and was twice the recipient of National Science Foundation Summer Fellowships.

Donald Joseph Belz is a member of Chi Epsilon and Omega Delta Phi.

This dissertation was prepared under the direction of the chairman of the candidate's supervisory committee and has been approved by all members of that committee. It was submitted to the Dean of the College of Engineering and to the Graduate Council, and was approved as partial fulfillment of the requirements for the degree of Doctor of Philosophy.

December 19, 1964

Thomas J. Martin Jr.
Dean, College of Engineering

Dean, Graduate School

Supervisory Committee:

W. A. Nash
Chairman

T. R. Elsayh

A. Johnston

T. Wernman

R. G. Blake